University of Illinois at Urbana-Champaign

ACRC

Air Conditioning and Refrigeration Center A National Science Foundation/University Cooperative Research Center

Assessment of Factors Contributing to Refrigerator Cycling Losses

P. J. Rubas and C. W. Bullard

ACRC TR-45 July 1993

For additional information:

Air Conditioning and Refrigeration Center
University of Illinois
Mechanical & Industrial Engineering Dept.
1206 West Green Street
Urbana, IL 61801

(217) 333-3115

Prepared as part of ACRC Project 30
Cycling Performance of Refrigerator-Freezers
C. W. Bullard, Principal Investigator

The Air Conditioning and Refrigeration Center was founded in 1988 with a grant from the estate of Richard W. Kritzer, the founder of Peerless of America Inc. A State of Illinois Technology Challenge Grant helped build the laboratory facilities. The ACRC receives continuing support from the Richard W. Kritzer Endowment and the National Science Foundation. The following organizations have also become sponsors of the Center.

Acustar Division of Chrysler
Allied Signal, Inc.
Amana Refrigeration, Inc.
Carrier Corporation
Caterpillar, Inc.
E. I. duPont Nemours & Co.
Electric Power Research Institute
Ford Motor Company
General Electric Company
Harrison Division of GM
ICI Americas, Inc.
Johnson Controls, Inc.
Modine Manufacturing Company
Peerless of America, Inc.
Environmental Protection Agency
U.S. Army CERL
Whirlpool Corporation

For additional information:

Air Conditioning & Refrigeration Center
Mechanical & Industrial Engineering Dept.
University of Illinois
1206 West Green Street
Urbana, IL 61801

217 333 3115

Abstract

Thermal mass effects, refrigerant dynamics, and interchanger transients are three factors affecting the transient and cycling performance of all refrigeration and air conditioning equipment. The effects of refrigerant dynamics, including refrigerant/oil solubility, off-cycle migration, and charge redistribution, were found to be the most important. These effects are quantified for a refrigerator instrumented with immersion thermocouples, pressure transducers, and microphones. The analytical methods, however, are applicable to other types of refrigeration and air conditioning systems, including those with capillary tube/suction line heat exchangers.

Table of Contents

List of Figures

List of Tables

Page

Chapter 1: Introduction and Literature Review

1.1 Purpose

The purpose of this research project is to obtain a detailed understanding of the cycling performance of refrigerator-freezers by identifying and quantifying the individual phenomena which degrade energy efficiency, relative to its steady state level. This is important because the Department of Energy uses a steady state simulation model as a basis for refrigerator standard setting, but tests for compliance under cycling conditions. Another objective of this research is to develop some insights about the need for a transient model, or whether a quasi-steady model could suffice with minor corrections. These goals are accomplished through the analysis of experimental data obtained with a typical household refrigerator (Amana model TC18MBL). It is a single evaporator, reciprocating compressor unit with a top mounted freezer compartment. Improvements made on the existing instrumentation will also be discussed.

1.2 Background and Previous Work

This research project builds on recent steady state work completed at the Air Conditioning and Refrigeration Center (ACRC) at the University of Illinois. Parameter estimation for the experimental refrigerator-freezer is described in detail by Reeves *et al* (1992), and a steady state model has been developed by Porter and Bullard (1992). An initial investigation of cycling performance degradation was provided by Staley *et al* (1992).

Previous work in the transient simulation of vapor compression systems falls into two categories: those that focus on the start-up transients associated with the first few minutes of an on-cycle, and those that model the continuous pull-down operation that makes up most of the remainder of the on-cycle. Examples of this type of work can be found in papers by Sugalski *et al* (1991), and Melo *et al* (1988). These simulations typically predict temperatures or pressures at various points within the system. However, they do not quantify the individual factors contributing directly relating to cycling losses.

The EPA Refrigerator Analysis Program, developed by Arthur D. Little, Inc. (ADL, 1992), estimates cycling losses as a linear function of cycling frequency. This was based on data from a single refrigeration loop used in a study by Janssen *et al* (1992), and may not be typical of other systems. ADL lists two major sources of cycling losses. First, the thermal load on the heat exchangers during the on-cycle is higher than the average load throughout the cycle, which leads to increased heat exchanger irreversibilities because of the larger temperature differentials. Second, during the off-cycle, refrigerant migrates from the condenser to the evaporator where it condenses and may release energy to the freezer air.

Refrigerant migration during the off-cycle has also been identified as one of the major components of cycling losses by other researchers. Wang and Wu (1990) indicate that the addition of a shut-off valve to prevent off-cycle migration can reduce overall energy use of a small air conditioner by four percent. Mulroy and Didion (1985) measured refrigerant migration in a split-system air conditioner by removing and weighing the refrigerant from the major system components during various points in the cycle. Their findings also indicate that refrigerant migration accounts for a significant portion of cycling losses.

The thermal mass of the system components has also been identified as a possible source of cycling losses. Staley *et al* (1992) state that the thermal mass of the refrigerator cabinet is not likely to be an important contributing factor to cycling losses, but the thermal mass of the compressor may improve transient performance by keeping discharge temperatures below steady state levels throughout the cycle.

1.3 Outline of This Report

Before beginning any transient analysis, the instrumentation on the existing test unit was upgraded. The heavy brass instrumentation blocks used during steady state data acquisition were removed in order to improve the response time of the thermocouples, and to prevent thermal lags. This is presented in detail in Appendix A.

Several of the parameter estimation techniques developed by Reeves *et al* (1992) were improved throughout the course of this study. The reverse heat leak technique for obtaining the overall heat transfer characteristics of the cabinet was refined. This was done by recreating the air flow patterns found inside the refrigerator-freezer during normal operation, and is detailed in Appendix B.

Chapter 2 focuses on the transients associated with the thermal mass of the major system components: the compressor, the cabinet, and the heat exchangers. Of all these components, the compressor's thermal mass is potentially the most important. The compressor shell temperature affects both the discharge temperature during the on-cycle and the solubility of the refrigerant in the sump oil throughout the cycle.

Chapter 3 analyzes the solubility of refrigerant in the compressor sump oil during cycling. The amount of refrigerant dissolved in the oil varies with temperature and pressure. This effect is potentially most important in compressors with high-side sumps, such as rotary compressors. Chapter 4 quantifies refrigerant migration during the off-cycle. Once the compressor shuts off, refrigerant from the condenser migrates through the capillary tube into the evaporator. The evaporator collects a surplus of charge that must be removed during the subsequent on-cycle before steady state performance can be approached. This redistribution of charge during the on-cycle is the focus of Chapter 5.

Chapter 6 examines the transients associated with the capillary tube-suction line heat exchanger. When the evaporator is low on charge and operates with a high level of superheat, the suction line becomes warmer. This tends to reduce the mass flow through the capillary tube, which delays the redistribution of mass into the evaporator.

Chapter 2: Thermal Mass Effects

2.1 Introduction

The purpose of this chapter is to begin an investigation of the transient behavior of a refrigerator, with an analysis of the thermal mass of the system components. Data for this analysis were taken in a 90 °F ambient room, with a charge of 12.5 ounces of R-12. The refrigerator was overcharged from its recommended 8 ounces for other testing, however qualitative results should be similar. The temperature control was set in its middle position to produce 60-minute cycles.

2.2 Comparison of Experimental Data

In order to make a performance evaluation, data from the cycling refrigerator must be compared to steady state data. The ambient air temperature and the evaporator inlet air temperature determine the operating conditions for a refrigeration system. Therefore, the average evaporator air inlet temperature over an entire cycle was compared with a steady state data point. These data are presented in Table 2.1. All of the data in the "Average Cycling" column were obtained by averaging the quantity for the entire cycle, including both the on- and the off-cycles. The data in the "Instantaneous Cycling" column were taken 23 minutes into the 35 minute on-cycle, at the time the evaporator air inlet temperature most closely matched the steady state value. By this time the refrigerator reached quasi-steady operation, and the sharpest transients associated with compressor startup had subsided. Air, refrigerant, and surface temperatures are denoted by TA, TR, and TS respectively.

Of immediate interest is the difference in the coefficient of performance (COP) for the two cases. The instantaneous COP in this case is actually greater than the steady state value; however, the average cycle COP is slightly lower as expected. Most of the transient losses occur during the first few minutes of the on-cycle as charge gets redistributed to its equilibrium location. The COP during the on-cycle starts lower and rises throughout the duration of the cycle (see Chapter 5).

Most of the data are surprisingly similar for both the steady state and cycling cases. One important difference between the two cases is the amount of superheat at the condenser inlet. This is due to the lower compressor discharge temperature for the cycling case. Also, throughout the on-cycle, the compressor shell temperature remains lower than the steady state value because of its thermal capacitance and the heat rejected during the off-cycle.

Table 2.1 Steady state and cycling performance

Measured Quantity	Steady State	Instantaneous Cycling	Average Cycling
TA:Evaporator Inlet (°F)	3.4	3.1	3.1
TA:Ambient (°F)	90.0	90.0	
TA:Condenser Inlet (°F)	96.4	96.0	
TA:Mid (°F)	101.6	100.7	
TR:Evaporator Exit (°F)	-11.3	-13.3	
TR:Evaporator Inlet (°F)	-12.9	-14.7	
TR:Condenser Exit (°F)	103.7	102.3	
Condenser Exit Subcooling (°F)	17.6	17.8	
TR:Condenser Inlet (°F)	198.6	190.8	
Condenser Inlet Superheat (°F)	77.0	70.4	
TR:Compressor Inlet (°F)	77.1	76.6	
TS:Compressor Shell (°F)	151.5	146.2	
Compressor Inlet Pressure (psia)	18.0	17.6	
Compressor Exit Pressure (psia)	176.0	173.3	
Mass Flow Rate at Cond. Exit (lbs/hr)	13.2	12.9	
Q Condenser (Btu/hr)	941	907	
Q Compressor (Btu/hr)	474	432	
Q Heaters (Btu/hr)	260	0	0
Q Evaporator (Btu/hr)	751	738	459
System Power (Btu/hr)	818	793	502
COP	0.92	0.93	0.91

2.3 Compressor Performance

Table 2.1 indicates that the total system power (which consisted of the compressor, evaporator fan, and the condenser fan) was 25 Btu/hr lower for the .cycling case. Since the power consumed by the evaporator and condenser fans remained constant for all data points, whether cycling or steady state, all of this difference must be attributed to the compressor. A First Law analysis explains the difference in measured compressor power, W_a, for the cycling and steady state cases. The energy balance on the compressor is given in Equation 2.1,

$$W_a = \dot{m}\Delta h + Q_{comp} + \frac{dU_{comp}}{dt} \qquad 2.1$$

where $\dot{m}\Delta h$ is the actual enthalpy change of the refrigerant across the compressor, Q_{comp} is the heat rejected by the compressor, and U_{comp} is the energy stored in the compressor shell. The relative magnitudes of the changes in these terms determine whether W_a increases or decreases during cycling.

At the instantaneous data point 23 minutes into the on-cycle, the suction inlet conditions were nearly identical. However, the discharge gas was cooler, possibly due to the compressor thermal mass. This reduced the first term in Equation 2.1 by about 16 Btu/hr.

The second term, Q_{comp}, can be calculated using Equation 2.2,

$$Q_{comp} = h_{comp}\Delta T \qquad 2.2$$

where h_{comp} is the overall compressor convective heat transfer coefficient, and ΔT is the temperature difference between the compressor shell and the surrounding air. The compressor heat transfer coefficient is calculated using 26 steady state data points taken at various ambient temperatures (for which Q_{comp} is known from a refrigerant side energy balance) as shown in Figure 2.1. The instantaneous value for Q_{comp} is 432 Btu/hr during cycling, or 42 Btu/hr less than the 474 Btu/hr observed during steady state operation. The compressor shell temperatures were 146.2 °F and 151.5 °F respectively, as shown in Table 2.1.

The thermal storage term can be evaluated using Equation 2.3,

$$\frac{dU_{comp}}{dt} = mc_p \frac{dT}{dt} \qquad 2.3$$

in which the thermal mass of the compressor shell, mc_p, is estimated to be 3 Btu/°F, and T is the compressor shell temperature. By measuring the rate of increase in the compressor shell temperature during cycling, the magnitude of the storage term is estimated to be 36 Btu/hr.

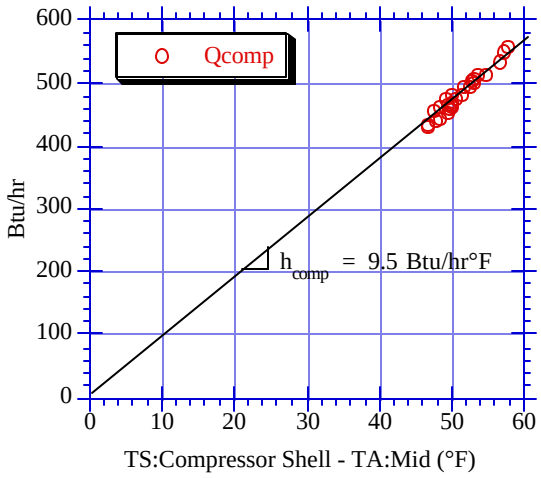

Figure 2.1 Compressor heat transfer coefficient

Summing the changes in all of the terms in Equation 2.4, W_a decreases by 22 Btu/hr for the cycling case, which nearly accounts for the 25 Btu/hr difference in measured power. Most of the error is attributed to the uncertainty of the thermal mass of the compressor, and in the power measurement.

A Second Law analysis can be used to determine the effect of thermal mass on compressor efficiency. The isentropic efficiency of the compressor, as defined by Equation 2.4,

$$h_s = \frac{W_s}{W_a} \qquad 2.4$$

can be calculated for all points during the on-cycle, and then compared to the steady state value corresponding to the same inlet air temperatures to the evaporator and condenser. The isentropic efficiency, h_s, is just the isentropic

work of compression, W_s, divided by the measured compressor power, W_a. The measured compressor power is compared to the power predicted by the compressor map in Appendix E. The isentropic work of compression is calculated using Equation 2.5,

$$W_s = \dot{m}(h_{in} - h_{out,s}) \qquad 2.5$$

in which $\dot{m}$ is the mass flow rate given by the compressor map (Admiraal, 1993), h_{in} is the enthalpy of the measured inlet state, and $h_{out,s}$ is the hypothetical enthalpy that would be obtained by isentropically compressing to the measured exit pressure. The turbine flow meter at the condenser exit cannot be used to measure the mass flow rate through the compressor during cycling; the mass flow rate through the compressor can be up to 10 percent greater than the mass flow rate at the condenser exit during the beginning of the on-cycle as charge collects in the condenser (see Chapter 5). The compressor efficiency for the on-cycle is plotted in Figure 2.2.

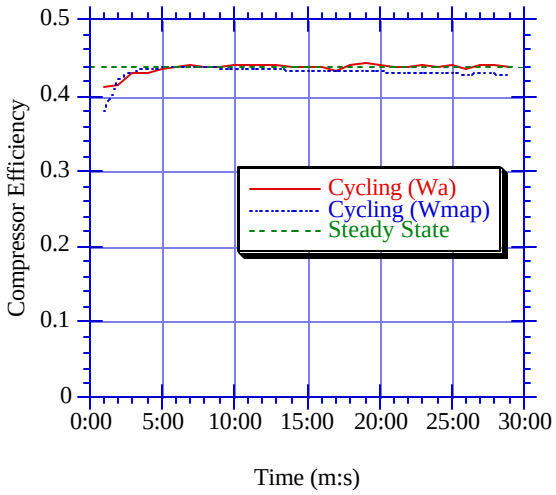

Figure 2.2 Isentropic compressor efficiency during cycling for 90 °F ambient case

During the first minute of the on-cycle, the mass flow rate through the compressor is not known with certainty because of the passage of liquid slugs, thus h_s is not shown. The instantaneous efficiency rose from 0.41 to 0.44 in the first 5 minutes, and then remained nearly constant for the remainder of the on-cycle. The corresponding steady state efficiency observed at the same evaporator and condenser air inlet temperatures, $h_{ss,}$ was 0.439. This is the same as the measured efficiency for most of the on-cycle. One reason for the initial increase in h_s is the decrease in compressor power, which occurs as a result of the decreasing suction pressure.

Also shown in Figure 2.2 is the isentropic compressor efficiency calculated using the compressor map power, h_{map}, instead of the measured power. The compressor map power, W_{map}, is a function of the measured compressor inlet and exit pressures, and was found to agree very well with W_a for steady state data taken in a 90 °F ambient room (see Appendix E). Therefore, W_{map} indicates how much power would be required by the compressor for the measured inlet and exit pressures, if the compressor were running at steady state. Any difference between W_{map} and W_a should therefore be attributable to the lower shell temperature during cycling. The steady state

efficiency, h_{ss} is higher than h_{map} at the point 23 minutes into the on-cycle because the inlet and exit pressures are slightly different as indicated in Table 2.1.

Since the compressor shell temperature increases throughout the on-cycle, approaching the steady state temperature, h_{map} should approach h_s rather than diverge as shown in Figure 2.2. One explanation for this anomaly is instrumentation error. W_{map} is very sensitive to the compressor inlet pressure; a constant 0.5 psia decrease in the pressure measurement would shift h_{map} upward by 0.01, placing it above h_s. Since the compressor inlet pressure is measured using the sum of three separate transducer readings with a combined uncertainty of ±0.8psia, a 0.5 psia offset is entirely possible. Also, W_a is determined by subtracting the evaporator and condenser fan powers from the total system power. The overall uncertainty in this measurement is ±4.1W (14 Btu/hr), which could also account for the difference between h_{map} and h_s.

A second set of cycling data was examined to see if the effect of the compressor thermal mass was similar. Figure 2.3 compares h_s and h_{map} for data taken in a 60 °F ambient room. This time, h_s was lower than h_{map} , and they converged throughout the cycle as expected. It appears that about half of the difference between h_s and h_{map} is accounted for by the 9W steady state offset in W_{map} as detailed in Appendix E. The compressor map, created from data obtained in 90 °F ambient conditions, under-predicts the compressor power at 60 °F ambient conditions by about 9W, independent of the pressure ratio. The compressor efficiency using the corrected map is also shown in Figure 2.3. Our data sets do not contain any steady state points that have similar inlet and exit pressures for comparison.

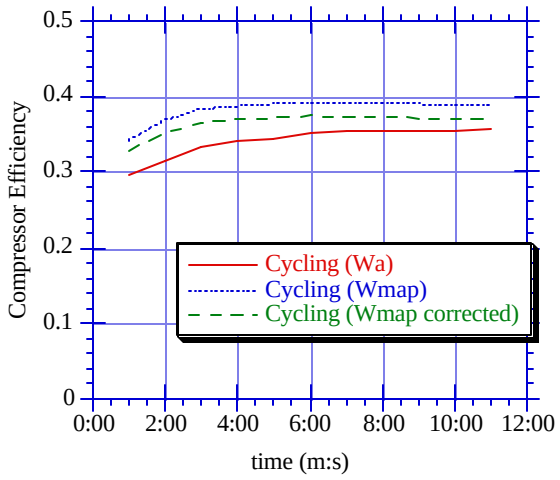

Figure 2.3 Isentropic compressor efficiency during cycling for 60 °F ambient case

Several other factors could contribute to the disagreement of h_{map} and h_s in Figures 2.2 and 2.3. At lower shell temperatures, the lubricating oil becomes more viscous, thus increasing friction between moving parts. This would tend to reduce h_s below h_{map}. Also, as the shell temperature varies, the mechanical clearances between parts changes, which could increase or decrease frictional losses.

One difference between the 60 °F and 90 °F ambient cases is that the compressor efficiency is much lower for the 60 °F case. This trend was apparent from our steady state data as shown in Appendix E, and can be explained

by the lower pressure ratios (which decrease the required compressor power) that are characteristic of lower ambient temperatures. An electric motor is usually less efficient when operating under a reduced load, thus the overall compressor efficiency is lower. Also, at lower temperatures, the lubricating oil is more viscous, thus frictional losses are increased.

In summary, the uncertainty in pressure and power measurements make it difficult to compare the observed cycling efficiency with the predicted steady state efficiency for the same inlet and exit pressures. More detailed tests are being planned to measure this effect.

A potentially more important factor is the effect of the compressor thermal mass on discharge temperature. This may have significant "downstream effects" on overall cycle performance under some operating conditions. For a case in which the condenser exit is saturated, a lower discharge temperature would decrease the condenser desuperheating area, allowing a larger two-phase area. For a given heat transfer, this would be accompanied with a decrease in condensing temperature, hence a higher COP. Unfortunately, our data sets do not include a cycling case with a two-phase condenser exit to verify this hypothesis. For cases like the one analyzed in this chapter with a subcooled condenser exit, the smaller desuperheating area is offset with a larger subcooled area, and the heat transfer rate and condensing area remain unchanged. This was analyzed using the ACRC2 steady state simulation model (Porter and Bullard, 1992). To simulate the effect of lower discharge temperatures caused by the compressor thermal mass, h_{comp} was varied for a case with 11 °F of condenser subcooling and 13 °F of evaporator superheat. The increasing compressor heat rejection (to the air and shell combined) was accompanied by an equivalent decrease in condenser heat transfer, which resulted in a nearly constant evaporator load. The model predicted that the COP and the total energy usage would remain unchanged despite the varying discharge temperature. This is consistent with the data presented here.

It appears from the linearity of Figure 2.1 that Q_{comp} can in fact be modeled as a function of compressor shell temperature. If this linearity holds for compressors in general, the parameter h_{comp} could be estimated using the dome temperature supplied with the compressor calorimetry data at the standard rating condition.

2.4 Heat Exchanger Thermal Mass

In theory, a refrigerator equipped with very massive heat exchangers, and a shut-off valve to prevent off-cycle migration, would approach the performance of a refrigerator with a variable speed compressor running at steady state (ADL, 1992). The massive heat exchangers would remain at a constant temperature, which would eliminate the irreversibilities due to the over- and under-shoot of the heat exchanger temperatures. The importance of the thermal mass of the heat exchangers used in the experimental refrigerator are examined in this section.

The lumped capacitance method is convenient for transient heat conduction problems in which the Biot number, as defined by Equation 2.6, is less than 0.1.

$$Bi = \frac{h_r L_c}{k} \qquad 2.6$$

The characteristic length for either heat exchanger, L_c, is just the tube wall thickness, h_r is the convection heat transfer coefficient (conservatively chosen as the refrigerant side coefficient), and k is the thermal conductivity of the heat exchanger material. The values used for this calculation are found in Table 2.2. In both cases, the Biot

number is far less than 0.1, hence the lumped capacitance assumptions are valid. With the lumped capacitance method, the importance of the thermal mass of the heat exchangers can be evaluated using their thermal time constants. Assuming a low Biot number, a solid that is subjected to a sudden temperature change will undergo approximately 2/3 of that temperature change in one time constant. After five time constants, the solid is considered to have reached equilibrium with its new surroundings. If the heat exchanger time constants are small compared to the cycling period of the refrigerator, then thermal mass effects can be neglected. The time constant for a heat exchanger is determined from Equation 2.7. The terms on the left side represent the energy entering the control volume from the refrigerant and air sides respectively. The term on the right side represents the energy stored in the heat exchanger itself. The subscripts r, a, and s refer to refrigerant side, air side, and surface properties respectively. The convection coefficients, h_r and h_a, are estimated using least squares techniques by Admiraal and Bullard (1993), and Cavallaro (1993). The heat exchanger areas, A_r and A_s, and the mass of the heat exchanger, m, are calculated from manufacturer's data. The specific heat of the heat exchanger material is c_p, and temperatures are denoted with T's. The solution of this differential equation results in a block of constants called the thermal time constant, τ, as given by Equation 2.8.

Table 2.2 Heat exchanger parameters

Parameter	Evaporator	Condenser
m (lbs)	3.35	3.95
L_c (ft)	2.33e-3	2.08e-3
k (Btu/hr ft °F)	136 (aluminum)	25 (steel)
c_p (Btu/lb °R)	0.22 (aluminum)	0.11 (steel)
h_r (Btu/h ft^2 °R)	75	60
h_a (Btu/h ft^2 °R)	5	5
A_r (ft^2)	4.07	2.02
Aa (ft^2)	17.25	6.40
Bi	1.3e-3	5.0e-3
τ (s)	6.8	10.2

$$h_r A_r (T_r - T_s) + h_a A_a (T_a - T_s) = mc_p \frac{dT_s}{dt} \qquad 2.7$$

$$t = \frac{3600 mc_p}{h_r A_r + h_a A_a} \qquad 2.8$$

This equation is solved for both the evaporator and the condenser using the values in Table 2.2. Even with conservative values chosen for the convection coefficients, the time constants are very small compared to a typical 30 minute on-cycle. From this calculation, it appears that the heat exchangers can respond rapidly to changes in their environment, and that their thermal mass has negligible effect on the refrigerator's performance.

2.5 Cabinet Thermal Mass and Conductance

Previous work at the ACRC suggests that the thermal mass of the refrigerator cabinet is not a significant contributor to cycling losses (Staley *et al*, 1992). The cabinet thermal mass has the same effect as food thermal mass; it just slows the decrease in air temperature. Since the average evaporator load is independent of cabinet mass, the

percent run-time and energy usage are unaffected. The EER averaged over a continuous quasi-steady pulldown is approximately equal to the EER at the midpoint. Thus, from a design standpoint, the thermal mass of the refrigerator cabinet is unimportant.

From a modeling standpoint, the cabinet thermal mass is very important in determining the length of the on- and off-cycles. As air circulates within the cabinet, it exchanges heat with the walls and shelves, thus the evaporator must also cool the cabinet. To illustrate the importance of this effect, the measured decline in evaporator air inlet temperature is compared with the temperature decline that would occur with a massless cabinet in Figure 2.4.

This hypothetical air temperature is obtained from the solution of Equation 2.9,

$$mc_v \frac{dT}{dt} = \dot{Q}_{air} \qquad 2.9$$

where m is the mass of the air inside the cabinet (1.4 lbs), c_v is the specific heat of air (0.173 Btu/lb-°F), T is the evaporator air inlet temperature, and $\dot{Q}_{air}$ is defined by Equation 2.10:

$$\dot{Q}_{air} = \dot{Q}_{evap} - UA_{frig}\Delta T_{frig} - UA_{frez}\Delta T_{frez} - P_{fan} \qquad 2.10$$

$\dot{Q}_{evap}$ is the observed evaporator heat transfer rate, as calculated from the air-side temperature difference across the evaporator. $UA_{frig}\Delta T_{frig}$ and $UA_{frez}\Delta T_{frez}$ represent the heat that leaks through the cabinet walls from the ambient air, and P_{fan} is the measured evaporator fan power. The air temperature increases initially because $\dot{Q}_{evap}$ is smaller than the cabinet loads during the beginning part of the on-cycle (see Chapter 5). Without the added thermal mass of the cabinet, the evaporator could have achieved its temperature set point in under 4 minutes, compared with 30 minutes for the actual on-cycle.

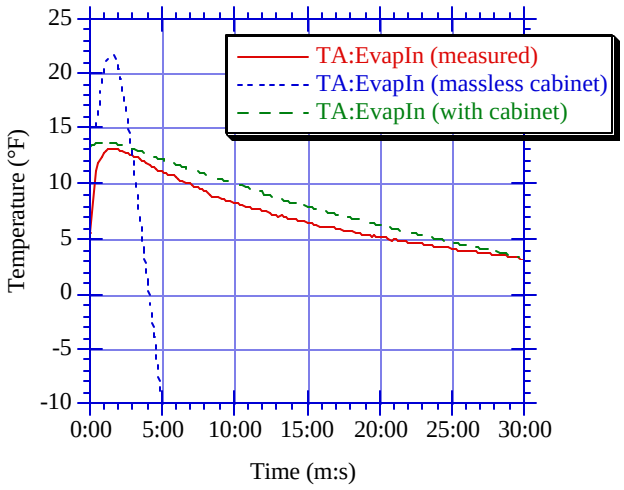

Figure 2.4 Cabinet thermal mass effect on evaporator inlet air temperature

To model the actual evaporator air inlet temperature decline, a cabinet thermal mass term is added to Equation 2.9. To simplify the calculations, the interior cabinet walls are assumed to follow the internal air temperature, and the outside cabinet walls remain at the ambient temperature. The temperature profile of the wall is

assumed to be linear, thus the average temperature of the cabinet is the average of the inside and outside air temperatures (Sugalski *et al*, 1991). With these simplifying assumptions, Equation 2.11

$$mc_v \frac{dT}{dt} + \frac{1}{2}\left(mc_p\right)_{cab} \frac{dT}{dt} = \dot{Q}_{air} \qquad 2.11$$

is used to model the cabinet, in which $(mc_p)_{cab}$ represents the thermal mass of the cabinet. Setting $(mc_p)_{cab}$ to 11 Btu/°F for this particular cabinet, the predicted evaporator air inlet temperature agrees with the measured evaporator air inlet temperature to within 2 °F, as shown in Figure 2.3. This calculation shows that the cabinet can be modeled using a simple lumped capacitance equation. Improvements can be made by realizing that some parts of the cabinet, for example the shelves, will undergo a larger temperature swing than the walls. They, like the various materials in the walls, can be modeled as a separate lumps for improved accuracy.

A major portion of the evaporator load for both steady state and cycling cases is the heat that leaks in through the cabinet walls from the ambient air. Therefore, it is important to investigate the effects of cycling on cabinet conductance. Both the fresh food and freezer compartment cabinet conductance's, UA_{frig} and UA_{frez} respectively, are usually determined using a reverse heat leak test, as detailed in Appendix B.

A common assumption of quasi-steady state models that predict transient performance is that the cabinet conductances are constant throughout the on- and off-cycles. During the off-cycle, the evaporator fan shuts off, and there is no longer forced convection in the freezer compartment. This leads to a decrease in UA_{frez}. UA_{frig} is less affected, since the fresh food compartment air flow rate is typically only 15 percent of the total evaporator fan air flow rate.

The affect on UA_{frig} and UA_{frez} of varying air flow rates was investigated by changing the air circulation fans used in the reverse heat leak tests. Using a 105 cfm muffin fan in the fresh food compartment resulted in a UA_{frig} of 1.011 W/°F. Switching to a 15 cfm fan dropped UA_{frig} by 11 percent to 0.898 W/°F. The results in the freezer compartment were more pronounced. Using the 105 cfm muffin fan in the freezer compartment (with the evaporator fan off) resulted in a UA_{frez} of 0.433 W/°F, and using the 45 cfm evaporator fan yielded a UA_{frez} of 0.530 W/°F. This 22 percent increase is attributed to the different air flow patterns behind the evaporator. This experiment shows that the internal air flow rates significantly affect the cabinet UAs. The decrease in cabinet conductance during the off-cycle may be as high as 20 percent, as evidenced by this experiment. To properly account for the cabinet load in a cycling model, different values for UA_{frig} and UA_{frez} are required depending on whether or not the evaporator fan is running.

Chapter 3: Refrigerant Solubility in Compressor Oil

3.1 Introduction

The purpose of this chapter is to estimate the magnitude of the movement of refrigerant to and from the oil in the compressor sump during transient operation. Refrigerant vapor enters the compressor shell and interacts freely with the oil in the sump before being compressed and expelled to the condenser. The amount of refrigerant dissolved in the oil changes as the pressure and temperature vary, thereby varying the amount of charge available to the rest of the system. The Grebner-Crawford model is used to estimate the solubility of the refrigerant in the oil for typical operating conditions. Following is an analysis for a case in which the refrigerator was charged with 12.5 ounces (360g) of R-12, and the ambient temperature was 75°F. This particular data is from an experiment in which the refrigerator was intentionally overcharged.

3.2 Pressure and Temperature Variations during Cycling

The variation of pressure with time was measured at the inlet to the compressor, and is shown in Figure 3.1. Initially the system was at thermodynamic equilibrium with the surroundings at 75°F. The refrigerator was turned on and the initial pulldown began. The following cycles were nearly uniform.

The temperature of the oil is more difficult to measure. Placing a thermocouple directly in the oil would require cutting a hole in the compressor shell which would be difficult to seal. Electrical interference from the strong magnetic fields generated by the motor may further complicate the reading. It is much more practical to measure the surface temperature of the compressor shell, or the refrigerant temperature leaving the compressor. For this purpose, four surface thermocouples were mounted to the compressor shell and insulated with 0.5 inches of foam, and an immersion thermocouple was placed at the compressor exit. These five temperatures are plotted during cycling in Figure 3.2. The refrigerant discharge temperature fluctuates over a wider range than the temperature of the compressor shell, which has a large thermal mass. Much of the temperature rise of the refrigerant is associated with the actual compression process, and it is less directly coupled to the sump. During an off-cycle the refrigerant is essentially at rest, losing heat to the surroundings. The copper tubing at the compressor exit acts as a fin and quickly cools the refrigerant within. For these reasons, it is probable that the oil temperature most closely follows the shell temperature. For the purposes of this model, the oil temperature is assumed to be an average of the four shell surface temperatures, which is plotted in Figure 3.3.

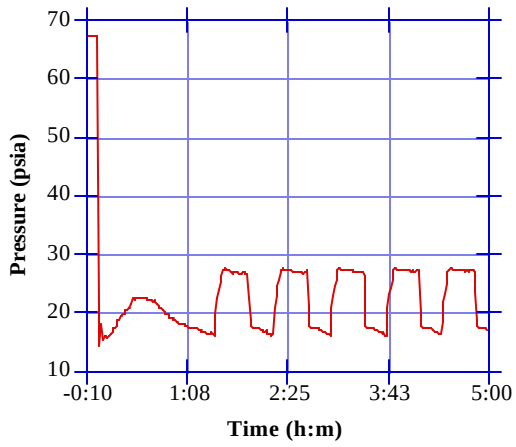

Figure 3.1 Pressure variation in compressor sump during cycling

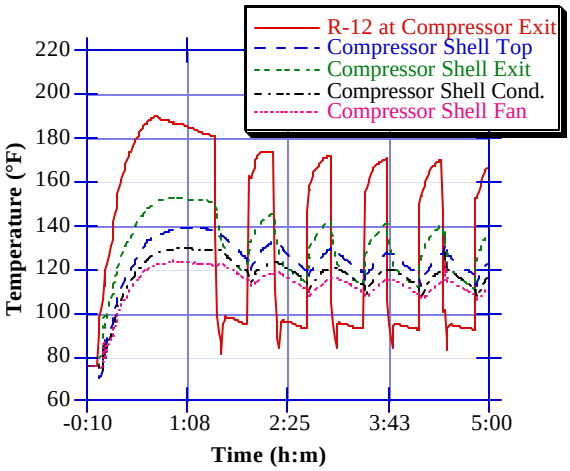

Figure 3.2 Compressor temperature during cycling

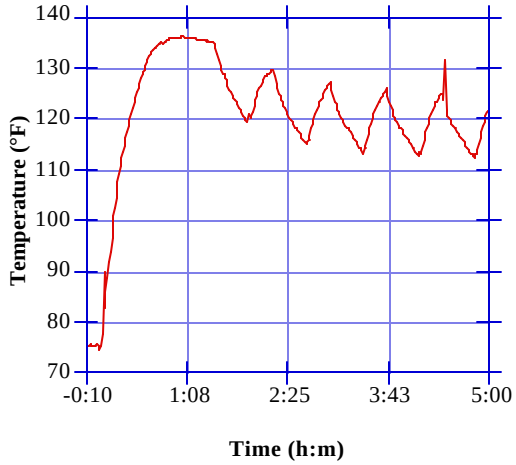

Figure 3.3 Average compressor shell temperature during cycling

3.3 Grebner-Crawford Refrigerant/Oil Mixture Model

The Grebner-Crawford equations (1992) empirically model an equilibrium mixture of refrigerant and oil. They are based on measurements taken at the ACRC for mixtures of R-12 and mineral oil over a range of temperatures and pressures which include refrigerator operating conditions. The equations, 3.1 through 3.4, take the form:

$$T^* = (1-w)(A + BP) \qquad 3.1$$

$$T^* = \frac{T - T_{sat}(P)}{T_{sat}(P)} \qquad 3.2$$

$$A = x_1 + \frac{x_2}{w^{1/2}} \qquad 3.3$$

$$B = x_3 + \frac{x_4}{w^{1/2}} + \frac{x_5}{w} + \frac{x_6}{w^{3/2}} + \frac{x_7}{w^2} \qquad 3.4$$

where T*, the nondimensional superheat for the mixture, is a function of the mixture temperature, T[°R], and the saturation temperature, $T_{sat}(P)$ [°R], of the pure refrigerant at the mixture vapor pressure, P [psia]. The liquid refrigerant mass fraction, w, is the mass of liquid refrigerant divided by the total mass of the liquid mixture. The constants x1 through x7 were determined by Grebner and Crawford from experimental data using least squares curve fits. For a mixture of R-12 and Naphthenic oil, the constants are given in Table 3.1.

Table 3.1 R-12/naphthene constants for Grebner-Crawford model

x_1	$-5.9927652 \times 10^{-3}$
x_2	4.1661510×10^{-2}
x_3	2.0046597×10^{-3}
x_4	$-3.2682848 \times 10^{-3}$
x_5	1.7368443×10^{-3}
x_6	$-2.8552230 \times 10^{-4}$
x_7	1.6092949×10^{-5}

The model is intended to predict equilibrium temperature (knowing w and P) or equilibrium pressure (knowing w and T). Using the model to predict pressure in an R-12/Naphthene mixture, for example, results in a root mean square error of only 2.23 psia over a range of 0 to 550 psia. The model can also be used to predict liquid refrigerant fraction (knowing T and P). Unfortunately, the accuracy here slips to ± 10% (the mass fraction is known to within ±0.10). Despite this, it should still be able to predict trends in refrigerant solubility in the compressor oil.

The compressor used in this analysis was a Tecumseh model AE1390V. It was lubricated by 13 ounces of grade 32 Naphthenic mineral oil (Sanvordenker, 1992). Knowing the mass of the oil and the mass fraction of refrigerant in the oil, the amount of refrigerant dissolved in the oil can be estimated using the Grebner-Crawford model. This is plotted for the various temperatures and pressures normally found in the sump in Figure 3.4. The plot looks nearly identical for R134a/ester oil mixtures.

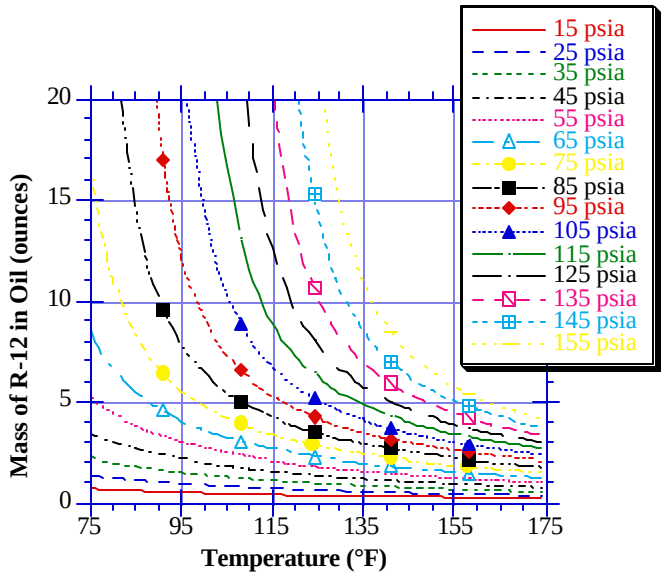

Figure 3.4 Solubility of R-12 in 13 ounces of naphthene

When at rest, the pressure and temperature were measured to be roughly 67 psia and 75°F. This corresponds to about 9 ounces of refrigerant, out of a total of 12.5 ounces, dissolved into the oil. During regular cycling, the pressure varied from roughly 15 to 30 psia and the temperature varied from roughly 110 to 130°F. This corresponds to about 1 ounce of refrigerant in the oil, thus 8 ounces of refrigerant boiled out of the oil during initial pulldown. During regular cycling, the pressure and temperature fluctuations were much smaller than during pulldown, so the amount of refrigerant entering and leaving the oil is not as large.

3.4 Refrigerant Movement from Compressor Oil during Regular Cycling

Using the average shell temperature and pressure variations introduced in section 3.2 the movement of refrigerant to and from the oil can be estimated. The mass of refrigerant in the oil for a typical pulldown and subsequent cycles is plotted in Figure 3.5.

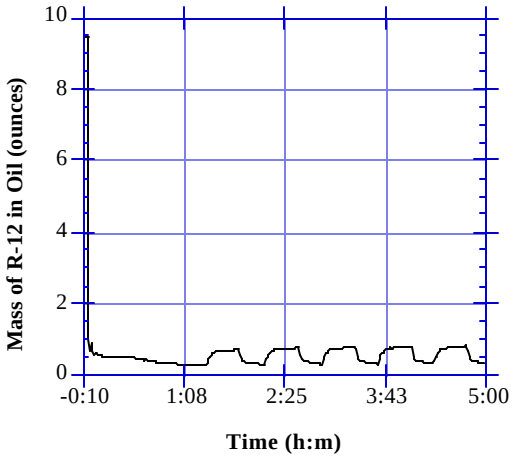

Figure 3.5 Mass of refrigerant in compressor oil during cycling

At the equilibrium initial conditions, the Grebner-Crawford model predicts that more than 9 ounces of refrigerant are dissolved in the oil. During the initial pulldown, nearly all of the dissolved refrigerant boils out of the oil, and only 0.3 ounces remain. The bulk of this fluid motion is caused by the temperature change as the compressor warms up, although the dropping pressure also contributes. This is easily shown by checking the model in Figure 3.4. During the following off-cycle, 0.4 ounces of refrigerant dissolve back into the oil. Again checking with Figure 3.4, it is clear that the solubility during regular cycling is primarily a function of pressure fluctuations, as the temperature is relatively stable. During the following cycles, the model predicts that 0.4 ounces of refrigerant move to and from the compressor oil.

3.5 Refrigerant Movement from Compressors with High Side Oil Sumps

Some compressors, including newer rotary models, have the oil sump on the high side. The oil sump in this case sees the compressor's discharge pressure, which may lead to different trends in refrigerant migration. Currently our data on a compressor with a high side sump is incomplete. The following analysis considers a hypothetical rotary compressor and uses the same data obtained from the low side compressor, with one exception. Since rotary compressors typically use about 25 % less oil than their rotary counterparts, the amount of oil is scaled down to 10 ounces. It is important to realize that the Grebner-Crawford model predicts liquid refrigerant mass fraction; changing the amount of oil just scales the mass of dissolved refrigerant in Figure 3.4 proportionally. This hypothetical configuration can be modeled using a similar analysis to determine if the magnitude of the movement is similar.

Since the evaporating and condensing temperatures of most refrigerators are similar, the pressures on either side of the compressor will also be similar. The variation of pressure on the compressor high side with time is measured and plotted in Figure 3.6. In comparison to the low side pressure plotted in Figure 3.1, the pressure swings on the high side are much larger. This should lead to larger movements of refrigerant into and out of the oil.

The temperature fluctuation of the oil is likely to be similar to the case when the oil sump is on the low side. As an approximation, the average compressor shell temperature, as plotted in Figure 3.3, can once again be taken as the oil's temperature. Previously, with a low side oil sump, temperature fluctuations had little effect on solubility due to the low pressures; however, the conditions at the high side of the compressor shell are such that the solubility is a strong function of both temperature and pressure (see Figure 3.4). It is now important to get an accurate measurement of the oil temperature to correctly model the solubility behavior.

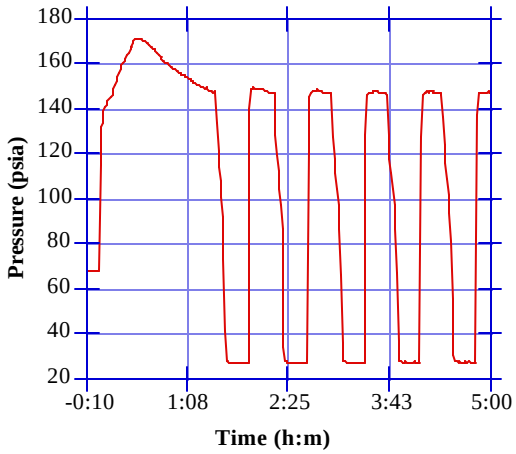

Figure 3.6 Pressure variation on compressor high side

Using the temperature and pressure fluctuations outlined above, the predicted mass of refrigerant dissolved in 10 ounces of oil is shown in Figure 3.7. During the initial pulldown, some of the refrigerant boils out of the oil as before, because of the temperature change. This time however, the pressure driving force opposes the temperature driving force, and less refrigerant is boiled out of the oil.

There is a strong discontinuity in the model's predictions just after the compressor turns on. The Grebner-Crawford equilibrium correlation yields an absurd result: more than 100% of the refrigerant is in the oil! This indicates that the system does not move immediately to an equilibrium state upon startup. As the compressor warms up, it tends to drive refrigerant out of the oil, and after 91 minutes the system reaches a near-equilibrium state in which about 6.8 ounces of refrigerant remain dissolved in the oil. The pressure at the end of this first on-cycle is 148.3 psia and the temperature is 135.5 °F. This can be compared with steady state data for which the pressure is 147.1 psia and the temperature is 133.3 °F. Since the steady state condition is by definition an equilibrium condition, we can accept the model's prediction that 7.3 ounces of refrigerant are dissolved in the oil. Perhaps this is why systems with rotary compressors require a larger refrigerant charge. When the compressor cuts off, there is again a sharp discontinuity, and about 10 minutes into the 25 minute off-cycle, the pressure and temperature approach an equilibrium that corresponds to about 0.5 ounce of refrigerant remaining in solution.

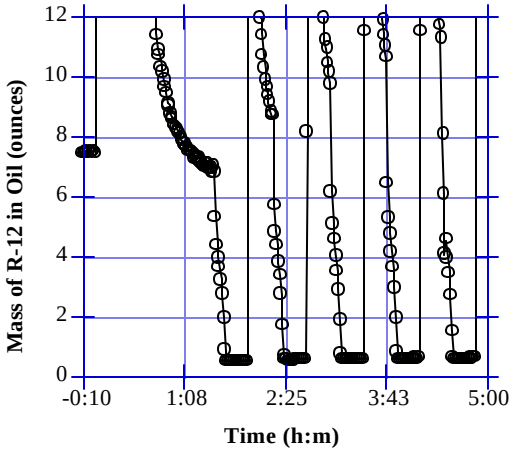

Figure 3.7 Refrigerant movement with high side sump

During the subsequent cycles, there are several immediate differences in the solubility trends. First, the direction of refrigerant movement is in the opposite direction for the two types of compressors. Second, with a high side sump, the refrigerant/oil mixture never reaches a steady state pressure and temperature during the on-cycle. Because of the compressor's thermal mass, the sump oil is still getting warmer at the end of the on-cycle. Thus it is not possible to know from available data with certainty whether the oil and refrigerant have reached equilibrium during the on-cycle. It is therefore possible that the actual movement of refrigerant to and from the oil is much smaller than the model's predictions, which represent the maximum possible magnitude. There could be a substantial difference in the amount of refrigerant dissolved in the oil for steady state conditions versus cycling conditions. Additional experiments are being designed to test this.

The worst case would occur if the adjustment to equilibrium is rapid. For the high side sump, as much as 6 ounces of charge move into and out of the oil during regular cycling, compared to 0.4 ounces for the low side sump. This is strongly related to the temperature of the oil. If the oil temperature were higher, the magnitude of refrigerant movement would be much smaller.

It is important to realize that the Grebner-Crawford model applies to equilibrium conditions. It is not intended to predict transient behavior of mixtures, which explains the large predicted mass swings immediately following compressor turn-on or turn-off in Figure 3.7. The mixture has not reached an equilibrium state and the model predictions are invalid. At the end of on or off cycles, it is believed that the mixture is approaching equilibrium, and that the model predictions, especially for the case of a low side sump, are correct. A future calculation to verify equilibrium conditions will commence shortly. Using void fraction formulae, the mass of refrigerant in all system components can be estimated. These will be summed with the refrigerant/oil model's predictions to get a total refrigerant mass. Of course this mass should be a constant, and its deviation would indicate nonequilibrium conditions.

Chapter 4: Refrigerant Migration

4.1 Introduction

When a refrigerator shuts off during its cycle, refrigerant migrates through the capillary tube from the condenser to the evaporator until the pressures equalize. This chapter will outline two possible modes of refrigerant migration and discuss the resulting heat transfer. Evidence will be presented to match data from an actual refrigerator to one of these modes. For this analysis, the refrigerator was intentionally overcharged from 8.5 to 11.5 ounces, however qualitative results should be similar for an optimally charged refrigerator. For the first data set, the temperature control was set to produce 60 minute cycles in a 90 °F ambient room. A second data set was obtained in a 60 °F ambient room using an 80W heat load to maintain a 60 minute cycle length.

4.2 Two Possible Migration Modes

The migration process can be modeled with two vessels, both of which contain two-phase refrigerant, connected by an adiabatic capillary tube. One is initially warm, representing the condenser, and the other is initially cold, representing the evaporator. During the off-cycle of a real refrigerator, a small amount of refrigerant actually leaves the evaporator via the suction line and dissolves into the compressor oil. For a refrigerator with a reciprocating compressor, this amount is estimated to be less than 0.4 ounces, hence it is neglected in this simple model.

The model is analyzed for two distinct migration modes. The first mode considers liquid migration, as shown in Figure 4.1, in which a liquid seal is maintained at the exit of the condenser. Since the pressure in the condenser is initially much greater than in the evaporator, liquid refrigerant begins to migrate through the capillary tube into the evaporator. This is shown by process a-b in the accompanying pressure-enthalpy diagram. Since the capillary tube is assumed to be adiabatic, the refrigerant undergoes no change of enthalpy as it travels through the capillary tube. Later during the off-cycle, with a lower condenser pressure and a higher evaporator pressure, the fluid follows path a'-b'.

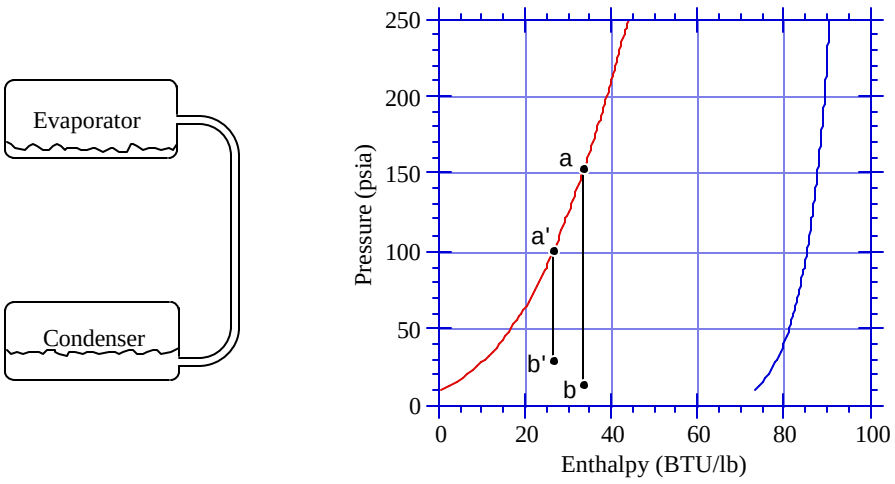

Figure 4.1 Liquid migration

The second migration mode is shown in Figure 4.2. Rather than maintaining a liquid seal at the condenser exit, vapor enters the capillary tube and migrates into the evaporator. The refrigerant initially follows path a-b in the accompanying pressure-enthalpy diagram, and at a later time step, path a'-b'. Clearly, the enthalpy of the refrigerant entering the evaporator is higher during vapor migration than it is for liquid migration. The energy implications of this difference will be analyzed in subsequent sections of this chapter.

The thermal mass of the suction line/capillary tube heat exchanger is estimated to be only 0.033 Btu/°R. During the off-cycle, the temperature of the evaporator end of the heat exchanger rises from 40 to 65 °F while the condenser end stays at a constant 90 °F. This corresponds to only 0.4 Btu change of energy stored in the heat exchanger. Some of this energy comes from the surrounding room air, and the remainder from the refrigerant flowing in the capillary tube. This is unlikely to cool the migrating refrigerant substantially, thus the assumption of an adiabatic capillary tube for the migration model is valid.

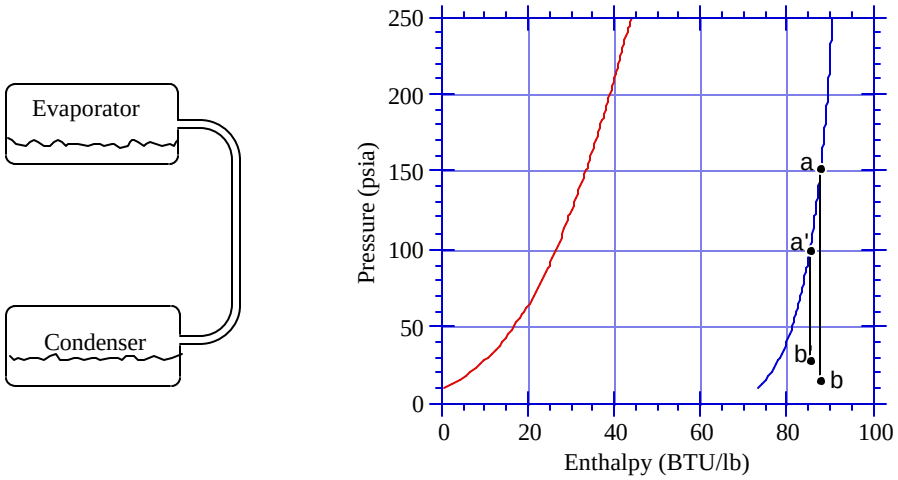

Figure 4.2 Vapor migration

4.3 Observed Migration Mode for the 90 °F Ambient Case

It is likely that the migrating refrigerant is initially liquid, and then vapor for the duration of the off-cycle. Because the test unit is overcharged, the condenser exit is nearly 20 °F subcooled at the end of an on-cycle. For this reason, it is assumed that for at least the beginning part of the off-cycle, liquid migration occurs. There is a filter drier just before the capillary tube, situated below the condenser exit, that is full of liquid. The heat flux through the filter drier is probably too small to vaporize this liquid, which must migrate before vapor migration can begin. The exit of the condenser is at the top; therefore as the compressor shuts off, it is likely that the liquid refrigerant would fall to the bottom of the condenser, and the vapor would rise to the exit. All subsequent migration would be vapor.

Figure 4.3 shows the observed refrigerant temperature at the evaporator inlet during a typical off- cycle, which begins at time 0:00 in the figure. Also plotted are the average freezer air temperature, and the maximum possible temperatures of entering refrigerant for both liquid and vapor migration modes. These are determined by equating the enthalpies at the inlet and exit of the capillary tube, and solving for temperature. The enthalpies at the inlet of the capillary tube are taken as saturated liquid or vapor at the condenser pressure. Relaxing the assumption of an adiabatic capillary tube would decrease the entering refrigerant temperature, since the vapor in the suction line

is initially cooler than refrigerant in the capillary tube. Also, taking into account the acceleration of the refrigerant through the capillary tube would further decrease the temperature of the entering refrigerant.

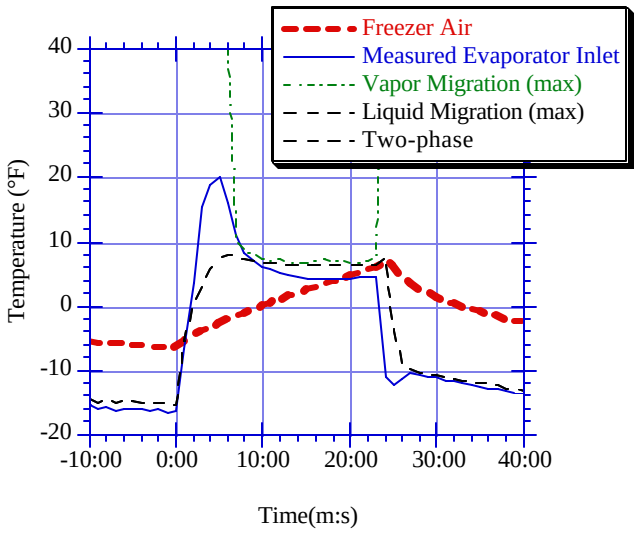

Figure 4.3 Evaporator inlet temperatures for 90 °F ambient case

It is interesting to note that the maximum entrance temperature for the liquid migration case is exactly the same as the two-phase temperature at the evaporator pressure. As saturated liquid migrates through the capillary tube, it remains two-phase, hence its temperature is uniquely defined by the pressure.

Almost immediately, the evaporator inlet and the two-phase temperatures become warmer than the surrounding freezer air, and stay that way for the rest of the off-cycle. Although they are not plotted, the air temperatures measured just above and below the evaporator are also lower than the refrigerant temperature at the evaporator inlet. During most of the off-cycle, these air temperatures are within 2 °F of the average freezer air temperature. Also not plotted is the evaporator exit temperature, which, like the inlet temperature, is warmer than the surrounding air temperature for most of the off- cycle. All of this indicates a reversal of heat transfer direction; during the off-cycle heat is transferred *from* the evaporator *to* the freezer air. This is consistent with the measurements made by Staley *et al* (1992) on a General Electric refrigerator.

Figure 4.4 shows the measured evaporator and condenser pressures during the same off-cycle. Since the pressures equalize about 8 minutes into the off-cycle, migration must be completed by this time. An interesting feature of the evaporator pressure is that it first increases as expected during the migration, but then drops slightly after the pressures have equalized. Since the mass in the evaporator is essentially fixed once the pressures have equalized, it is likely that this small drop in pressure is caused by the heat transfer from the evaporator to the freezer air.

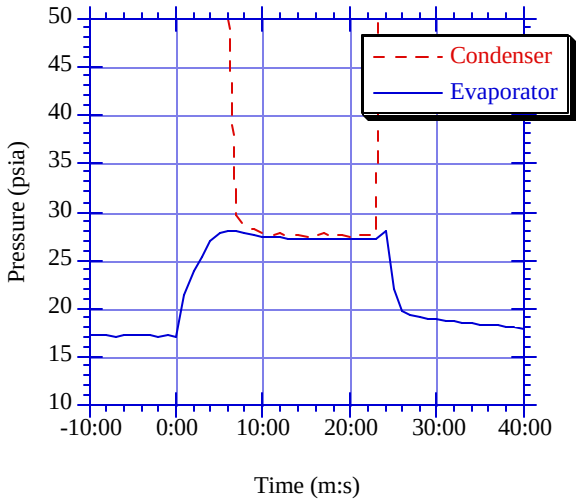

Figure 4.4 Condenser and evaporator off-cycle pressures for 90 °F ambient case

For the initial two minutes of the off-cycle, the data are consistent with the hypothesis of liquid migration, since the maximum possible entering refrigerant temperature is slightly greater than the measured evaporator inlet temperature. For the next six minutes only vapor migration is possible, because the maximum refrigerant temperature for liquid migration is below the measured inlet temperature. After this point, the pressures in the evaporator and condenser have essentially equalized, and migration ceases.

Figure 4.5 shows condenser temperatures during the off-cycle. The air temperature is measured near the middle of the condenser at the rear of the refrigerator. Air temperatures are measured at other locations near the condenser, and the trends are similar. The measurement of the refrigerant temperature at the condenser inlet is heavily influenced by the compressor shell temperature because of the proximity of the thermocouple. The compressor shell (and hence the refrigerant at the condenser inlet) is warmer than the surrounding air throughout the off-cycle. This results in heat transfer *from* the compressor and this part of the condenser *to* the air. At the exit the opposite is true. The air is warmer than the condenser, so heat is transferred *to* this section of the condenser. Also plotted in Figure 4.5 is the saturation temperature at the condenser pressure. Once the compressor stops, the contents of the condenser are believed to be two-phase until a majority of the charge has migrated out. After this point, the remaining refrigerant is superheated vapor. Within two minutes of the start of the off-cycle, the two-phase temperature falls below the surrounding air temperature. This indicates that heat is being transferred from the air to the refrigerant as it boils. The temperature in no part of the condenser falls as low as the two-phase line in Figure 4.5 indicates, because the condenser becomes superheated before the pressure equalizes with that of the evaporator.

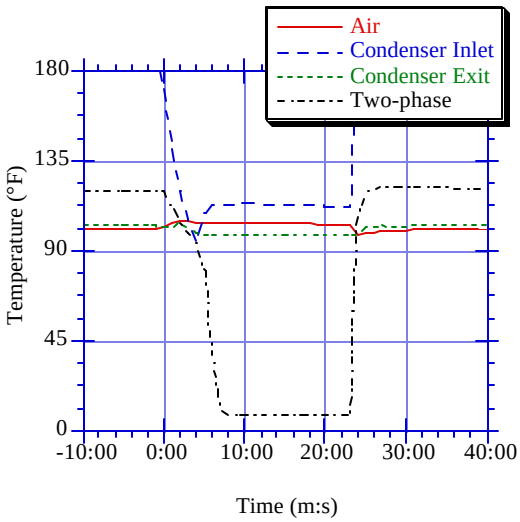

Figure 4.5 Condenser off-cycle temperatures for 90 °F ambient case

It is difficult to describe the temperature of the condenser during the off-cycle because it is non-uniform. The coolest part is probably the bottom set of tubes, where the liquid part of the two-phase refrigerant drains. Unfortunately, no thermocouples exist in this location to verify this. The thermal mass of the compressor keeps the inlet the warmest part of the entire condenser, and the thermal mass of the condenser itself is probably what keeps the exit at a nearly constant 100 °F. Migrating vapor traveling through the condenser coil has a low heat capacity, and is unlikely to alter the coil temperature significantly. Instead, the vapor temperature rises from its saturation temperature to match the coil temperature at the exit. This was verified through a surface temperature measurement at the condenser exit.

These observations provide solid evidence for vapor migration during the period from two to eight minutes into the on-cycle, but don't indicate which mode(s) of migration occur for the first two minutes. At least initially, it is likely that liquid migration occurs because the condenser exit is subcooled at the end of the on-cycle. From geometrical considerations, it is estimated that as much 1 ounce of liquid migrates before the liquid seal is broken, and vapor migration takes over. A computer simulation has been written to model the migration process, and it is presented in the next section.

4.4 Migration Simulation

The mass of refrigerant initially in the condenser and evaporator is estimated using the Zivi void fraction correlation, along with the assumption of a linear change in quality through the heat exchanger. The largest uncertainty in this estimate is in determining the volume of subcooled liquid at the end of the condenser. This is the largest contributor to total charge, and is also the most difficult to estimate. As a starting point, it is assumed that the condenser contains 5.8 ounces of charge, and the evaporator contains 1 ounce.

The mass flow rate through the capillary tube is modeled separately for liquid and vapor migration modes. For liquid migration, a curve fit was created from a detailed finite difference capillary tube model (Peixoto, 1993). It assumes that the liquid entering the capillary tube is saturated, and that the flow is choked. This is normally the case

during regular refrigerator operation, and is initially true during the off-cycle migration process. Under choked flow conditions, the receiver (evaporator) pressure has no effect on the mass flow rate. For a given capillary tube geometry, the mass flow rate becomes solely a function of the condenser pressure, as given by Equation 4.1,

$$\dot{m}_{vap} = -1.987 + 0.121P_{cond} - 0.000234P_{cond}^{2} \qquad 4.1$$

where $\dot{m}_{vap}$ is the mass flow rate in lbs/hr, and P_{cond} is the condenser pressure in psia.

For the case of vapor migration, Fanno flow conditions are assumed. The vapor is isentropically accelerated from rest in the condenser to some velocity at the entrance to the capillary tube, where Fanno flow (adiabatic flow through a constant area duct with friction losses) begins. The flow can be checked for choked conditions by assuming a Mach number of one at the exit, and then using Fanno relations determine the pressure at the exit. If this pressure is greater than the receiver (evaporator) pressure, the flow is choked, and the Mach number at the exit is indeed one. If the calculated pressure is lower than the receiver pressure, then the flow must be subsonic, and the exit Mach number must be less than one. The latter case is found to be true for the entire range of inlet and exit pressures measured for the off-cycle migration process. In order to estimate the mass flow rate under these conditions, Equations 4.2.a - 4.2.d must first be solved simultaneously to obtain an entrance Mach number. The length of the

$$\frac{fL}{D} = \left(\frac{g+1}{2g}\right)\ln\left(\frac{1+\frac{g-1}{2}M_{out}^2}{1+\frac{g-1}{2}M_{in}^2}\right) - \frac{1}{g}\left(\frac{1}{M_{out}^2} - \frac{1}{M_{in}^2}\right) - \left(\frac{g+1}{2g}\right)\ln\left(\frac{M_{out}^2}{M_{in}^2}\right) \qquad 4.2.a$$

$$P_{cond} = P_{in}\left(1+\frac{g-1}{2}M_{in}^2\right)^{\left(\frac{g}{g-1}\right)} \qquad 4.2.b$$

$$\left(\frac{P_{out}}{P_{in}}\right) = \left(\frac{M_{in}}{M_{out}}\right)\left(\frac{1+\frac{g-1}{2}M_{in}^2}{1+\frac{g-1}{2}M_{out}^2}\right)^{\frac{1}{2}} \qquad 4.2.c$$

$$P_{out} = P_{evap} \qquad 4.2.d$$

capillary tube, L, is measured to be 125.5 inches long, and its diameter, D, is given by the manufacturer to be 0.033 inches. The friction factor, f, is estimated from a Moody diagram to be 0.03 throughout most of the flow conditions. The specific heat ratio, γ, is assumed to be a constant 1.104 for all calculations. Throughout this discussion, the subscript "in" represents the inlet to the capillary tube, likewise the subscript "out" represents the exit. The subscript "cond" refers to conditions within the condenser where the fluid velocity is neglected, and "evap" refers to similar conditions in the evaporator. Finally, Mach numbers are designated with M, absolute pressures with P, and absolute temperatures with T. Equations 4.2.a and 4.2.c are Fanno flow relations, and Equation 4.2.b is an isentropic relation. Equation 4.2.d represents a condition that must be met in order to have subsonic (unchoked operation) flow throughout the capillary tube.

Equations 4.3 - 4.5 can now be solved sequentially to determine the mass flow rate.

$$\left(\frac{T_{cond}}{T_{in}}\right) = \left(1 + \frac{g-1}{2} M_{in}^2\right) \qquad 4.3$$

$$c_{in} = \sqrt{gRT_{in}} \qquad 4.4$$

$$\dot{m}_{vap} = \frac{r_{in} M_{in} c_{in} A}{3600} \qquad 4.5$$

Equation 4.3 is an isentropic relation which provides the temperature at the inlet to the capillary tube. This is used in Equation 4.4 to calculate the speed of sound, c_{in}, of the refrigerant vapor. The ideal gas constant for R-12, R, is 411 $ft^2/sec^2°R$. Finally, the mass flow rate of the refrigerant vapor, $\dot{m}_{vap}$, is calculated in Equation 4.5 in lbs/hr. In this equation, the density of refrigerant vapor entering the capillary tube, ρ_{in}, is a thermodynamic function of temperature and pressure, which have already been determined. The cross-sectional area of the capillary tube entrance in ft^2 is denoted by A.

A better estimate of the refrigerant temperature entering the evaporator can be obtained from Equation 4.6, which is also a Fanno relation.

$$\left(\frac{T_{out}}{T_{in}}\right) = \left(\frac{1 + \frac{g-1}{2} M_{in}^2}{1 + \frac{g-1}{2} M_{out}^2}\right) \qquad 4.6$$

Once liquid and vapor mass flow rates are known functions of temperature and pressure, a model can be developed to study refrigerant migration. Using the basic schematic presented in section 4.2, an unsteady energy balance, Equation 4.7, can be written for the condenser control volume. The internal energy of the control volume, $E_{cond\ cv}$, can be written as shown in Equation 4.8. The condenser in this particular refrigerator is made entirely of steel, and all of its

$$\frac{dE_{cond\ cv}}{dt} = \dot{Q}_{cond\ cv} - \dot{m} h_{out} \qquad 4.7$$

$$E_{cond\ cv} = m_{steel} c_p T_{cond} + m_{ref} u_{ref} \qquad 4.8$$

dimensions are known from the manufacturer. This makes it a simple matter to calculate its thermal mass, $m_{steel}\, c_p$, which in this case is 0.435 Btu/°F. T_{cond} is the temperature of the saturated refrigerant, and also represents the temperature of the condenser itself. Even though the condenser temp erature is clearly non-uniform, using T_{cond} to represent both the refrigerant and coil temperatures significantly simplifies the calculations. The mass of refrigerant in the condenser, m_{ref}, is initially 0.375 lbs., and it decreases as the refrigerant migrates out of the condenser. The internal energy of the refrigerant, u_{ref}, is a thermodynamic function of temperature and quality, x, which is in turn defined by equation 4.9,

$$x = \frac{V - m_{ref} v_{liq}}{m_{ref} \left(v_{vap} - v_{liq}\right)} \qquad 4.9$$

which is derived from the definition of quality. The volume of the vessel (in this case the condenser), V, is estimated from manufacturer specifications to be 0.007666 ft^3, and the specific volumes of saturated liquid and vapor refrigerants, v_{liq} and v_{vap} respectively, are thermodynamic functions of temperature and pressure. The rate of heat transfer to the condenser is represented by $\dot{Q}_{cond\ cv}$, which is given by Equation 4.10. Since the condenser fan is not running during the off-cycle,

$$\dot{Q}_{cond\ cv} = UA_c(T_{air} - T_{cond}) \qquad 4.10$$

the dominant heat transfer mode is natural convection. The heat transfer coefficient, UA_c, is estimated from natural convection relations to be 1.65 Btu/hr °F (Cavallaro and Bullard, 1994). The air temperature surrounding the condenser, T_{air}, varies slightly as evidenced by Figure 4.5, however in order to simplify calculations, it is taken to be constant at 105 °F. The enthalpy of the exiting refrigerant is given by h_{out}. Since it is observed that the condenser exit temperature is nearly constant at 100 °F, h_{out} is calculated at this temperature for the vapor migration case. This is an attempt to correct for the non-uniform temperature of the condenser. During liquid migration, however, the enthalpy is calculated differently. Initially the exit enthalpy is calculated as subcooled liquid, in this case at 100 °F. After the compressor shuts off, liquid refrigerant collects in the bottom set of condenser coils. It mixes to attain uniform temperature (the saturation temperature at the condensing pressure) and the subcooling is eliminated.

By setting P_{cond} equal to the saturation pressure at T_{cond}, these equations define the mass flow rate and the change in condenser temperature and pressure with time for either mode of refrigerant migration. The most important factor, however, is the amount of energy transferred to the freezer compartment during the migration process. This is estimated using Equation 4.11, which is similar to Equation 4.7. This time, the control volume is drawn around the evaporator.

$$\frac{dE_{evap\ cv}}{dt} = -\dot{Q}_{evap\ cv} + \dot{m}h_{in} \qquad 4.11$$

The terms in this equation are defined in a similar manner as those used in the condenser control volume. It is unimportant to know whether the energy added to the evaporator control volume ($\dot{m}\,h_{in}$) is stored within evaporator ($\dot{E}_{evap\ cv}$) or transferred to the surrounding air ($\dot{Q}_{evap\ cv}$). Figure 4.3 shows that the evaporator is essentially in thermal equilibrium with the surrounding air by the end of the off-cycle. This means that the heat transfer between the evaporator and the air is negligible. Therefore, the energy penalty associated with migration is just the integral over time of $\dot{m}\,h_{in}$.

All of these equations were solved using a program which is listed in Appendix C. All derivatives are taken numerically, and all thermodynamic properties are curve fits of table data written in the form of functions. The block of simultaneous equations describing Fanno flow were solved using a Newton-Raphson subroutine. The initial values for temperature and pressure were those measured at the end of an on-cycle. It is assumed that 1 ounce of liquid migrates initially, and that all subsequent migration is vapor. A plot of the model's predicted condenser pressure variation with time is compared with the measured pressure in Figure 4.6.

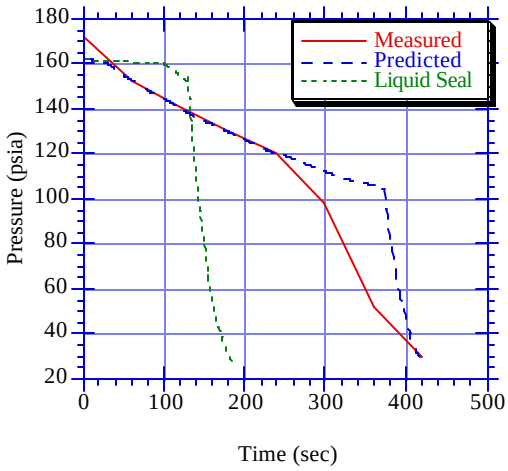

Figure 4.6 Predicted and measured condenser pressure during off-cycle

Also shown in Figure 4.6 is the hypothetical case for which a liquid seal is maintained as long as possible at the condenser exit.

The migration model agrees very well for the beginning of the off-cycle, however it does not predict the transition from a two-phase to a superheated condenser well. The model shows this transition as a distinct change of slope at 375 seconds. In the actual condenser this transition may not be as sharp. While the model assumes that the entire condenser is of uniform temperature, it actually varies in different locations as discussed previously. Although no thermocouples exist near the middle of the condenser, it is likely that the temperature here drops substantially lower than in the rest of the condenser as the refrigerant inside boils off. This non-uniformity is difficult to model, and is likely to be a major source of error in the model. Also, once the liquid in the condenser is gone, the pressure is determined using a constant compressibility factor in conjunction with the ideal gas law. The compressibility factor used in the calculations is 0.83, and is obtained from a generalized compressibility chart for temperatures and pressures typically measured at the condenser exit during the off-cycle. This is likely to introduce significant error in the pressure calculation, since the compressibility factor varies substantially with superheat near the saturation dome. A better curve fit for pressure as a function of density and pressure could alleviate this shortcoming. There is excellent agreement during the vapor migration portion of the model while the condenser is clearly two-phase. This helps to verify the estimated mass flow rate, and the total mass that has migrated, which is important in determining the energy losses associated with the migration process. Also, the model indicates that vapor migration is likely to begin very early in the off-cycle.

If a liquid seal is maintained as long as possible, the migration process takes place much faster because the mass flow rate of liquid is much higher than the mass flow rate of vapor. To model this case, liquid migration is assumed until only 1 ounce of refrigerant remains in the condenser. At this point, the liquid seal is broken and vapor migration takes over, as indicated by the change in slope 100 seconds into the off-cycle. After about 40 seconds of vapor migration, the condenser is no longer two-phase, and the pressure drops rapidly to its equilibrium value. A perfect liquid seal would allow all but 0.15 ounces to migrate as liquid, but this is probably unattainable in practice. The horizontal tubing used in the condenser is likely to allow refrigerant vapor to migrate well before all the liquid is

gone. If the exit was at the bottom of a vertical tube, it might be possible to maintain the liquid seal for almost the entire off-cycle.

4.5 Energy Penalty Resulting From Migration for 90 °F Ambient Case

The migration model quantifies the energy penalty associated with the migration process for both of the cases described in the previous section. For the case in which vapor migration dominates, nearly 29 Btu's are added to the freezer. Part of this leaves as heat transferred from the evaporator to the surrounding air, while the remainder adds to the internal energy of the refrigerant inside the evaporator. For the case in which a liquid seal is maintained as long as possible, only 15 Btu's are transferred into the freezer compartment. These numbers are quite small compared with the overall cabinet load for one complete on/off-cycle, which for these operating conditions is estimated to be 397 Btu. Using this as a reference, the migration process represents an additional 7% load for the predominantly vapor migration case, and an additional 4% load for the predominantly liquid migration case.

It is possible that this additional load could be eliminated using a shutoff valve at the entrance to the capillary tube. This would prevent any charge from leaving the condenser during the off-cycle, and would maintain high- and low-side pressures nearer to their equilibrium values. At the very least, the condenser exit could be oriented such that a liquid seal is maintained for the majority of the migration process. This could nearly halve the energy penalty.

4.6 Observed Migration Mode for 60 °F Ambient Case

Data from the same refrigerator cycling in a 60 °F ambient room were also analyzed to see if the migration process was similar. A constant 80W heat load was added during both the off- and the on-cycles to the refrigerator and freezer cabinets in order to lengthen the cycle time to 60 minutes. By the end of the on-cycle, the condenser exit was subcooled by 4 °F, so it is again likely that liquid migrates for at least the beginning portion of the off-cycle. Figure 4.7 shows the observed refrigerant temperature at the evaporator inlet as well as the maximum possible temperatures for migrating liquid and vapor during an off-cycle beginning at time 0:00. Also plotted is the average freezer air temperature. The figure shows that liquid migration is only possible for the first 30 seconds of off-cycle, after which the measured evaporator inlet temperature is higher than the maximum possible liquid migration temperature. Thus for the 60 °F ambient case, vapor migration begins much earlier in the off-cycle. Since the vapor migration flow rate is much lower than the liquid flow rate, the migration time is longer for a given amount of charge. This can be seen in Figure 4.8, which shows the condenser and evaporator pressures during the off-cycle. The pressures equalize about 10 minutes into the off-cycle, as opposed to 8 minutes for the 90 °F ambient case.

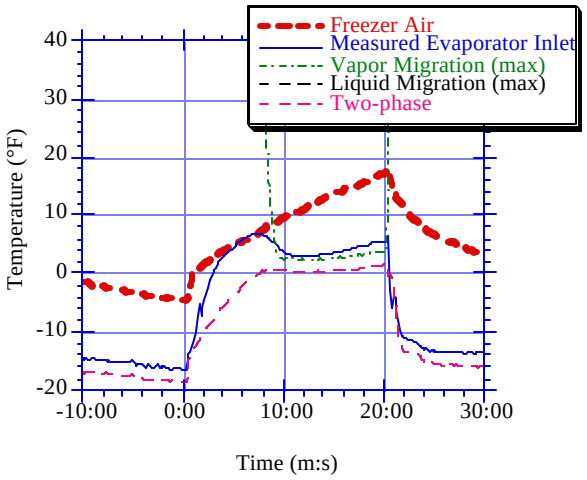

Figure 4.7 Evaporator inlet temperatures for 60 °F ambient case

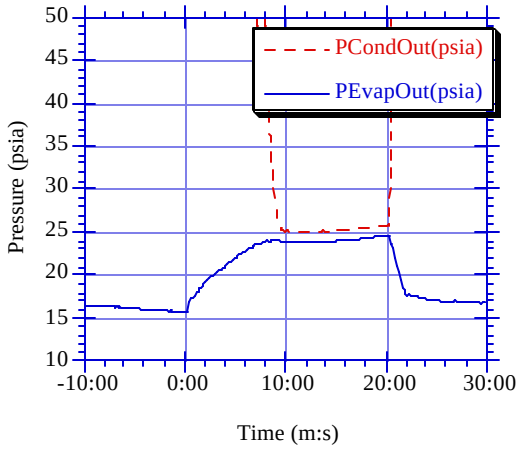

Figure 4.8 Condenser and evaporator off-cycle pressures for 60 °F ambient case

An important difference between the two data sets is the direction of heat transfer during the off-cycle. Figure 4.7 shows that the freezer air temperatures is at all times greater than the evaporator temperature. This results in heat transfer *from* the air *to* the refrigerant in the evaporator, producing a beneficial cooling effect. Since the evaporator inlet refrigerant temperature is near the saturation temperature for the second half of the off-cycle, it is likely that the refrigerant is boiling during this time.

4.7 Energy Implications Resulting From Migration for 60 °F Ambient Case

Just as for the 90 °F ambient case, the migrating refrigerant adds between 15 and 30 Btu's to the evaporator during the off-cycle. The important difference is that this time the energy is not transferred *to* the freezer air, rather the refrigerant continues to absorb heat *from* the freezer during the entire off-cycle. When this surplus refrigerant is pulled out of the evaporator at the beginning of the on-cycle, all of the 15 to 30 Btu's added during the migration process are removed with it. Since the direction of heat transfer is into the refrigerant, all of the energy brought into the evaporator by migrating refrigerant stays in the refrigerant. When the surplus charge is removed as liquid or as

vapor, all of the stored energy plus the energy energy added to the refrigerant from the freezer air is removed at the same time. This additional refrigerating effect results in an efficiency increase. The refrigerating effect, ΔQ_{refrig}, can be estimated using Equation 4.12, where UA_e is the natural convection coefficient

$$\Delta Q_{refrig} = \int UA_e \left(T_{air} - T_{evap}\right) dt \qquad 4.12$$

of the evaporator. T_{air} and T_{evap} are the air and evaporator temperatures, and t is the time during which heat transfer occurs. Using a rough estimate of 2 Btu/h °R for UA_e, the total refrigerating effect is only 3 Btu, which is negligible compared to the 362 Btu cabinet load for the entire cycle. Thus, the migration process itself does not impose an additional load on the refrigerator for the 60 °F ambient case.

4.8 Conclusions

The migration process itself does not appear to have much impact on the overall evaporator load during cycling. However, having the surplus charge in the evaporator at the beginning of the on-cycle may slow the return to a quasi-steady operating condition. The next chapter will focus on the phenomena associated with startup. It is believed that the evaporator is nearly evacuated by the compressor as it first starts, and that the starved evaporator causes a loss of efficiency until charge is redistributed through the capillary tube. If this is true, having extra charge in the evaporator at the beginning of the on-cycle may reduce this starving effect. Conversely, if a surplus of charge remains in the evaporator during the initial part of the on-cycle, it will take longer for the evaporating temperature to drop. This too will decrease efficiency as it takes longer for the evaporator heat transfer rate to reach its quasi-steady value.

Chapter 5: Charge Redistribution

5.1 Introduction

Immediately following the compressor startup, several transients keep the refrigerator from operating at steady state. One reason for this is the maldistribution of charge throughout the system. By the end of the off-cycle, the evaporator may contain up to 6.5 ounces of saturated refrigerant (see Chapter 4). About 5.5 ounces of this must be redistributed to the other components in order to achieve quasi-steady state operation. As the compressor starts up again, this charge may begin to leave the evaporator gradually as a vapor, or as slugs of saturated liquid. If slugs of liquid refrigerant are drawn out of the evaporator into the compressor, the evaporator may reach its steady state charge rather quickly. Furthermore, if the slugs vaporized upon entering the warm compressor, the resulting lower discharge/suction pressure ratio would increase the mass flow rate through the compressor, thus further accelerating the redistribution of charge to the condenser. However, if the slug flow from the evaporator is too vigorous, it could starve the evaporator of refrigerant. This would result in high superheat levels and an accompanying loss of capacity until a steady state distribution is reached.

If there is an accumulator at the evaporator exit and it is oriented properly, much of the liquid refrigerant could be retained in the evaporator, and only vapor would exit. In this case the liquid would have to be boiled off resulting in heat transfer from the freezer air to the refrigerant. The cooling effect, ΔQ, can be calculated using Equation 5.1. The mass of the liquid refrigerant

$$\Delta Q = m h_{fg} \qquad 5.1$$

in pounds is given by m, and h_{fg} is the enthalpy of vaporization at the evaporating temperature, in this case 68 Btu/lb. If, for instance, 5 ounces of refrigerant are boiled off during the first part of the on-cycle, the cooling effect is 21 Btu. During that time, however, there will only be vapor leaving the evaporator, and it will take longer for the saturation pressure and temperature to drop, and for the rate of heat transfer from the freezer air to increase.

The instantaneous amount of charge in the evaporator is determined by the difference between the flow rates into and out of the evaporator. The flow rate into the evaporator from the capillary tube is initially much lower than its steady state value, because the exit of the condenser contains superheated vapor at the beginning of the on-cycle. The vapor flow rate is approximately one fourth the liquid flow rate through the same pressure difference (see Chapter 4). As the charge builds up in the condenser, the exit quality drops and the mass flow rate through the capillary tube increases.

This chapter examines the redistribution of charge and its effects on refrigerator performance. For this experiment, the refrigerator was intentionally overcharged from 8.5 to 11.5 ounces; however, qualitative results should be similar for an optimally charged refrigerator. Data were taken in both a 90 °F and a 60 °F ambient room, and analyzed separately.

5.2 Observed Charge Redistribution Mode for 90 °F Ambient Case

Data from the refrigerator were examined to determine which mode of charge redistribution occurred. With an ambient temperature of 90 °F, the evaporator exit was immediately saturated upon startup, and remained that way for the duration of the on-cycle. As the excess refrigerant gradually boiled out, the evaporator was able to maintain a

two-phase exit. The data show that it is unlikely that all of the charge slugged out as a liquid. This would have starved the evaporator of refrigerant, and forced it to operate with a high level of superheat until more charge was brought in through the capillary tube.

Figure 5.1 shows the refrigerant temperature at the evaporator exit, as well as the saturation temperature at the measured exit pressure, for an on-cycle beginning at time 0:00. If the measured evaporator exit temperature differed from the saturation temperature, it would indicate that either superheated vapor or subcooled liquid must have flowed out of the evaporator. Except for the pressure spike about 10 seconds into the on-cycle, the refrigerant temperature closely followed the saturation temperature. Unfortunately, this does not indicate whether liquid or vapor exited the evaporator. However, it is likely that the pressure spike was caused by a slug of liquid passing the pressure tap. During a subsequent cycle, a pressure spike was also observed, but this time it was in the opposite direction. The data acquisition system used in this study was limited to a ten-second sampling interval. For future work it will need to be modified to obtain a finer resolution to better observe pressure spikes and other sharp transients.

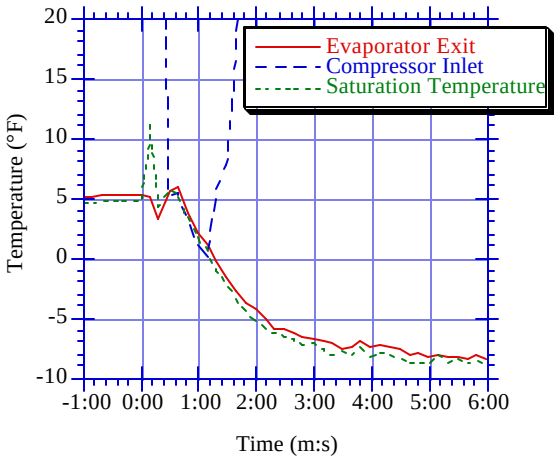

Figure 5.1 Evaporator exit temperature at beginning of on-cycle in a 90°F room

In order to gain additional insights, a small microphone was placed near the accumulator exit to check if liquid slugs could be heard passing it. The microphone was embedded in a small hole in a piece of foam insulation such that its face was pressed against the tubing. This assembly was wrapped with a second layer of foam to provide further insulation from outside noise. The microphone was fed into a standard audio tape recorder which was turned on just before the beginning of an on-cycle.

The dominant sounds on the tape are the compressor and fan noises; however, with the aid of an audio equalizer, much of this can be filtered out. During the beginning portion of the off-cycle, liquid refrigerant can be heard splashing inside the evaporator. This activity ceases approximately midway into the 25 minute off-cycle. During the first ten seconds of the on-cycle, several quick gurgling noises can be heard which probably indicate the movement of liquid slugs. Between 40 and 60 seconds into the on-cycle, sharp pinging or knocking sounds are heard, possibly the result of liquid entering the compressor. This is supported by Figure 5.1, which shows that the

refrigerant at the compressor inlet is saturated at that time. The information obtained by the microphone supports the hypothesis that several liquid slugs exited the evaporator, although it does not confirm it, nor does it give any indication of how much liquid might have slugged out before vapor began to flow.

The refrigerant temperature at the compressor inlet dropped from nearly 100 °F to 5 °F during the first 30 seconds of the on-cycle. The refrigerant became saturated and remained that way until the capillary tube/suction line heat exchanger (interchanger) began to work (about 70 seconds into the on-cycle), after which the refrigerant in the suction line was clearly superheated. During the first 60 seconds of the on-cycle, the suction line surface temperature dropped nearly linearly from 60 °F to 5 °F at the evaporator end, and from 90 °F to 40 °F at the compressor end. The energy stored in the interchanger was primarily removed by the refrigerant flowing through the suction line, since the mass flow rate through the capillary tube is initially very low.

During the first 30 seconds of the on-cycle, both the refrigerant and the suction line surface temperatures changed rapidly. Much of the refrigerant that exited the evaporator must have been vapor since its temperature rose as it cooled the suction line. The thermal mass of the interchanger, 0.033 Btu/°F, is estimated by multiplying its mass by the specific heat of copper. In order for the abrupt temperature change to have occurred, the refrigerant must have absorbed about 1 Btu from the interchanger during the first 30 seconds of the on-cycle. Assuming a typical mass flow rate of 15 lbs/hr (based on the compressor map at the measured evaporating and condensing pressures), about 2 ounces of saturated refrigerant vapor could have flowed from the evaporator. In order for this vapor to absorb the 1 Btu of energy stored in the interchanger, it would have to undergo an average temperature change of 55 °F. This can be compared to the time-averaged temperature change that was measured during the first 30 seconds of the on-cycle, which for this case was 47 °F. Since the measured temperature change is very close to the temperature change that would have to occur for vapor-only flow, it is believed that most of the refrigerant exited the evaporator as saturated vapor. This is further confirmed by comparing the observed refrigerant-side convective heat transfer coeficient with the theoretical vapor-only coefficient obtained from the Dittus-Boelter equation. The details of this calculation are found in Appendix D.

Between 30 and 60 seconds into the on-cycle, the refrigerant temperature at the compressor inlet stabilized to the saturation pressure, while the suction line surface temperature continued to drop rapidly as it rejected another 1 Btu of stored energy. During this period, liquid slugs evidently exited the evaporator and vaporized as they absorbed energy from the suction line. If saturated vapor were exiting the evaporator, it would have superheated and continued to rise in temperature, which is inconsistent with the data in Figure 5.1.

Evidently, during the first 30 seconds of the on-cycle, most of the charge leaving the evaporator was saturated vapor. For the next 30 seconds, predominantly liquid slugs exited the evaporator, and they vaporized as they continued to remove heat from the suction line. One explanation for this is that initially the liquid slugs were trapped by the accumulator, and mainly saturated vapor flowed through the suction line. After the accumulator filled up, liquid began to spill out, and several slugs flowed into the suction line. About 70 seconds into the on-cycle, the interchanger began to work, and any refrigerant flowing through the suction line was superheated before it could reach the compressor.

5.3 Evaporator Performance for 90 °F Ambient Case

For a transient analysis, the evaporator heat transfer rate in Btu/hr, $\dot{Q}_{evap}$, is most easily calculated using an air side energy balance as indicated by Equation 5.2. The volumetric flow

$$\dot{Q}_{evap} = \frac{60\dot{V}c_{p\,air}\Delta T}{v} \qquad 5.2$$

rate of the evaporator fan, $\dot{V}$, is known to be a constant 68 cfm (Admiraal and Bullard, 1993), and the specific volume of air, v, is calculated using the ideal gas law. The specific heat of air, $c_{p\,air}$, is taken at the average air temperature around the evaporator, and ΔT is the measured air temperature difference through the evaporator in °F.

The evaporator heat transfer rate is plotted for the first fifteen minutes of the on-cycle in Figure 5.2. $\dot{Q}_{evap}$ climbed rapidly for the first four minutes before it approached its average quasi-steady value of about 552 Btu/hr. The surplus of charge in the evaporator caused it to operate with a saturated exit throughout the duration of the on-cycle.

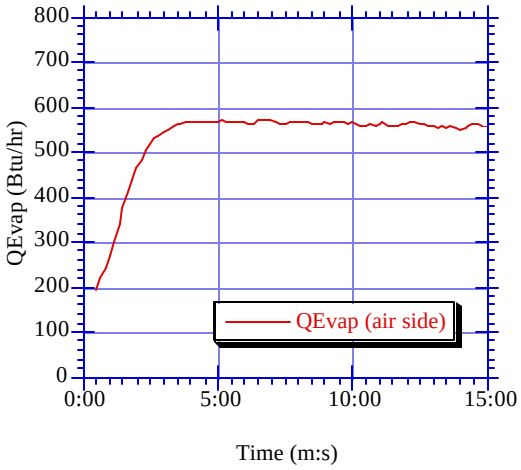

Figure 5.2 Evaporator capacity for 90 °F ambient case

Initially, the evaporator was in thermal equilibrium with the surrounding air as shown in Figure 5.3. With no temperature difference, no heat transfer can occur. This explains the low evaporator capacity at the beginning of the on-cycle. As the surplus charge slowly boiled off, the pressure and the saturation temperature of the evaporator declined, and heat transfer between it and the air increased. Warm air drawn in from the fresh food compartment caused the initial upward spike in evaporator inlet air temperature. Thereafter, the air temperatures declined monotonically for the rest of the on-cycle.

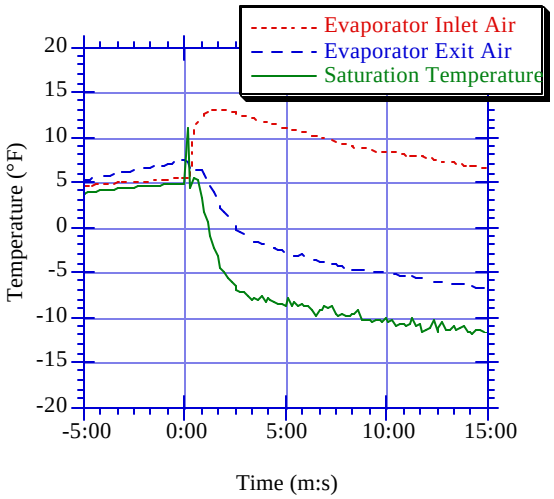

Figure 5.3 Evaporator air temperatures for a 90°F ambient case

The evaporator heat transfer rate became nearly constant within four minutes of startup, despite the declining air temperature. This represents the balance points of the system, which are defined by the governing set of simultaneous equations. From this point forward, the temperature difference between the incoming air and the evaporator remained nearly constant. The heat transfer coefficient was also constant, since the entire evaporator was always flooded. The system maintained a constant evaporator heat transfer rate by dropping the evaporating temperature.

The loss in capacity can be quantified by comparing the average evaporator heat transfer rate with the "steady state" value. Over the entire on-cycle, the evaporator removed heat at an average rate of 539 Btu/hr. By ignoring the first four minutes of the on-cycle during which the evaporator capacity was rising rapidly, the average quasi-steady value of $\dot{Q}_{evap}$ was 552 Btu/hr. This indicates a 2.3 % loss in capacity as a result of the startup transient. The lower initial capacity would not be considered an efficiency loss if the system power was correspondingly lower during the beginning part of the on-cycle. However, Figure 5.4 shows that the opposite was true. The compressor power declined sharply at the beginning of the on-cycle because the evaporating pressure was dropping. Although the condensing pressure was increasing during this time, which by itself would have increased power consumption, the low-side pressure had a stronger influence on compressor power than the high-side pressure. This is verified by the compressor calorimetry supplied by the manufacturer.

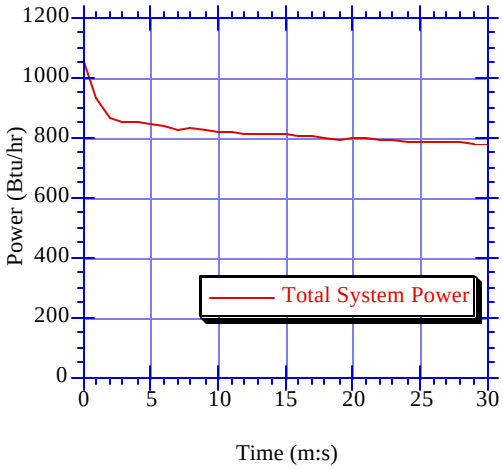

Figure 5.4 Total system power for 90 °F ambient case

The COP during the on-cycle is plotted in Figure 5.5. The plot shows that nearly all of the degradation of COP occurred during the first four minutes of the on-cycle as the charge was being redistributed.

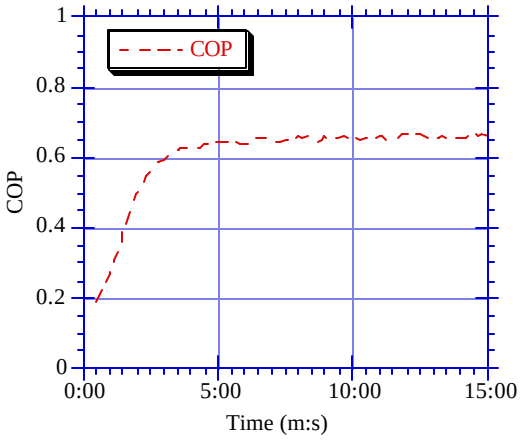

Figure 5.5 COP for 90 °F ambient case

5.4 Observed Charge Redistribution Mode for 60 °F Ambient Case

Data from the same refrigerator in a 60 °F ambient room were also examined in order to observe differences in the charge redistribution. To lengthen the cycle time, a constant 80W heat load was distributed between the freezer and fresh food compartments throughout the on- and off-cycles. Without this additional heat load, the on- and off-cycles were too short to reach quasi-steady state operation, and the charge did not have enough time to migrate and redistribute fully. An alternative method to lengthen the cycles would be to add a large thermal mass to the freezer compartment to slow the system's response. Figure 5.6 shows the evaporator exit temperature, as well as the saturation temperature at the measured exit pressure, for an on-cycle beginning at time 0:00. This time the refrigerant at the exit of the evaporator was significantly superheated at the end of the off-cycle. This may have been the result

of the particular arrangement of liquid and vapor within the evaporator. Since the freezer air temperature was warmer than the evaporator during the off-cycle, heat transfer from the air evidently superheated pockets of vapor near the exit of the evaporator (see Chapter 4). At the start of the on-cycle, the exit immediately became two-phase as it did in the previous case. This in itself cannot confirm whether liquid, vapor, or both flowed from the evaporator upon startup.

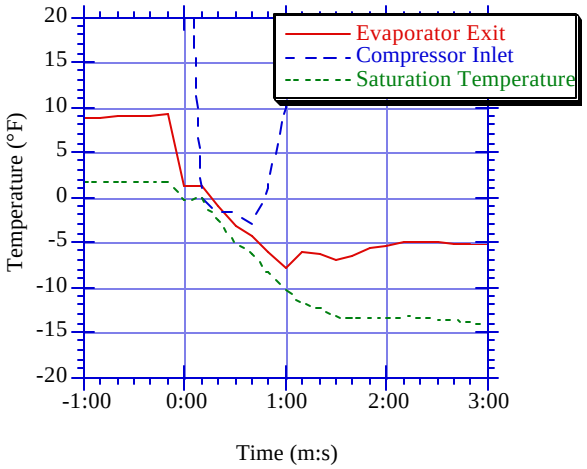

Figure 5.6 Evaporator exit temperature at beginning of on-cycle in a 60°F room

Once again a microphone was employed to gather additional insight about refrigerant flow throughout the cycle. This time, the refrigerant was heard splashing inside the evaporator throughout the entire 20 minute off-cycle. Since the evaporator and condenser pressures equalized, and the contents of the condenser became entirely superheated (both within 10 minutes), it is likely that the off-cycle migration process was completed by the time the 30 minute on-cycle began. The charge that had migrated was evidently boiling and rearranging itself within the evaporator coils. A different tape recorder was used this time to record the microphone signal, and unfortunately the fidelity suffered. It became much more difficult to pick out the sound of flowing refrigerant even with the aid of an audio filter. Once the compressor started, faint gurgling sounds were heard to indicate that liquid slugs were leaving the evaporator. The sharp tapping sounds heard in the 90 °F ambient case were no longer discernible. Future tests should employ a very high quality audio tape recorder with a noise filter to remove some of the microphone hiss. An audio equalizer with 10 or more bands would be helpful to filter out compressor noise, which dominated the tape. It is unlikely that further insulating the microphone would reduce the noise level, since the sound is transmitted directly through the metal tubing.

As it did before, the refrigerant at the compressor inlet became saturated, although for a shorter time than in the 90 °F case. This is another indication that slugs of liquid may have been drawn out of the evaporator.

5.5 Evaporator Performance for 60 °F Ambient Case

Using Equation 5.2, the evaporator heat transfer rate is plotted for the first 30 minutes of the on-cycle in Figure 5.7. This time, the evaporator heat transfer rate rose for only two minutes before it reached full capacity. The heat transfer rate actually dropped slightly before approaching its average quasi-steady value of 999 Btu/hr. Figure

5.8 shows the evaporator air and refrigerant temperatures for this particular cycle. The refrigerant temperature at the evaporator inlet was the same as the saturation temperature throughout the on-cycle, indicating that at no time was the entire evaporator filled with superheated vapor; there was always sufficient charge to maintain a two-phase inlet. It is likely that as the compressor started, it drew out enough charge to cause the exit to become superheated. Then, the level of superheat continued to rise as the compressor mass flow rate led the capillary tube mass flow rate, and the evaporator charge continued to decline. This is verified by Figure 5.9, which shows the mass flow rates into and out of the condenser. These were obtained from a compressor map and a turbine flow meter respectively. The turbine flow meter reading was corrected using a steady state offset of +1 lb/hr (Admiraal and Bullard, 1993). Since the flow rate into the condenser was greater than the flow rate out, the condenser must have been collecting charge. This is further verified by Figure 5.10 which shows a concurrent increase in condenser subcooling. Near the middle of the on-cycle, the capillary tube mass flow rate (as measured by the turbine flow meter) rose above the compressor mass flow rate, and charge began to accumulate back into the evaporator, thus reducing the level of superheat to its quasi-steady value of about 3 °F. The evaporator was unable to operate with a saturated exit because the additional charge it required was in the subcooled zone of the condenser.

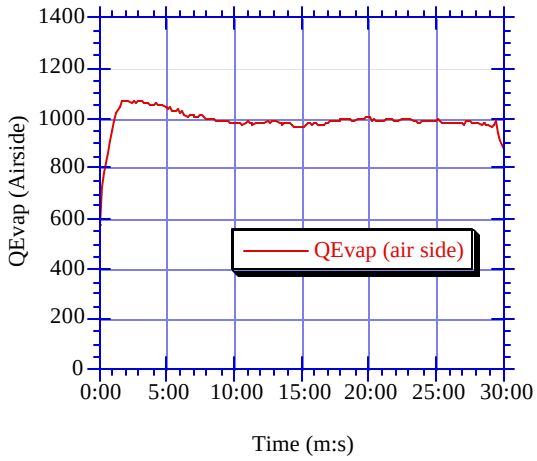

Figure 5.7 Evaporator capacity for 60 °F ambient case

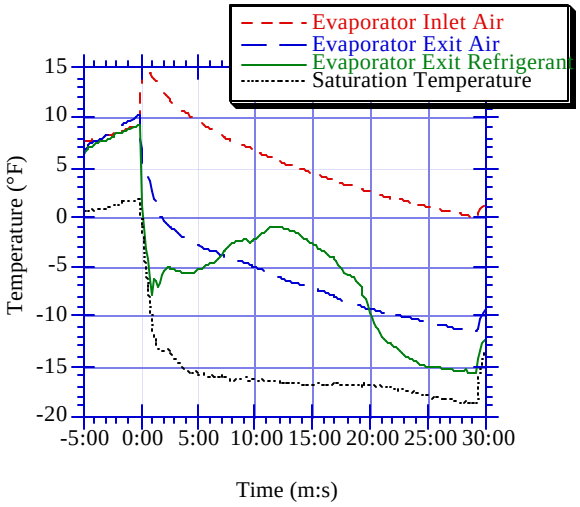

Figure 5.8 Evaporator air temperatures for a 60°F ambient case

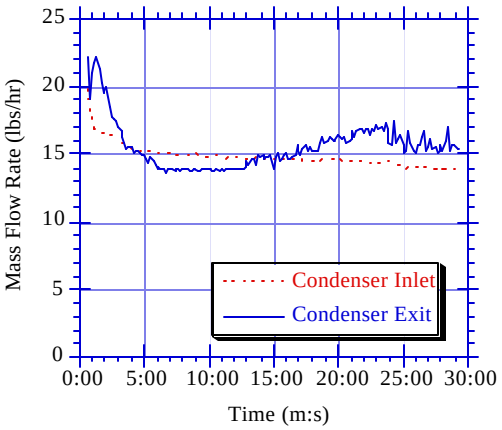

Figure 5.9 Condenser mass flow rates for 60 °F ambient case

After the initial transients, the evaporator heat transfer rate again remained nearly constant as a result of the balance points of the system. The declining level of superheat counteracted the declining temperature difference between the evaporator and the incoming air. As the superheated area decreased, the two-phase area grew, corresponding to an increase in the overall evaporator heat transfer coefficient. These opposing effects maintained a nearly constant evaporator heat transfer rate.

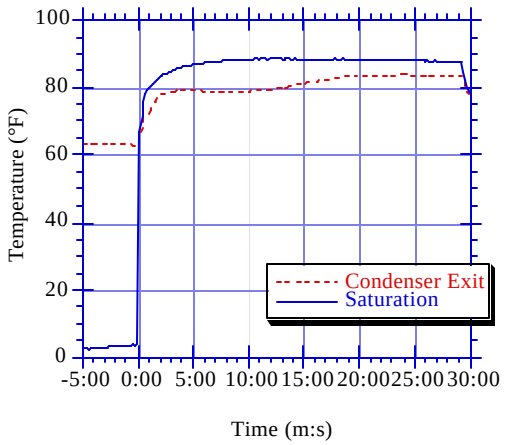

Figure 5.10 Condenser subcooling for 60 °F ambient case

Figures 5.8 through 5.10 indicate that the charge was redistributing throughout the on-cycle as the system tried to maintain a balance point. The bulk of the charge redistribution (about 5 ounces) occurred during the first two minutes of the on-cycle as the evaporator emptied. After this was completed, there was a slower charge redistribution back into the evaporator (up to 0.5 ounces), which reduced the level of superheat. This secondary redistribution had a much smaller effect on evaporator performance, as shown in Figure 5.7. It is unlikely that the addition of the electric heaters used to provide the constant 80W heat load changed the characteristics of the redistribution. Since the heat was well distributed throughout the cabinet, it was no different than the heat that leaked through the cabinet walls from the ambient air. Thus, these conclusions should apply equally well for a refrigerator without heaters.

The loss in evaporator capacity can be quantified as before. In this case, the evaporator reached full capacity in only two minutes, compared to four minutes for the 90 °F ambient case. The average evaporator heat transfer rate over the entire on-cycle was 488 Btu/hr, compared with the average quasi-steady value of 491 Btu/hr. This translates into only a 0.6 % loss in capacity. The COP for this on-cycle is plotted in Figure 5.11. The plot clearly shows most of the degradation in COP occurred during the first two minutes as the evaporator heat transfer rate was low and the system power was high. The plot also shows a noticeable degradation in COP in the middle of the on-cycle when the evaporator had a high level of superheat.

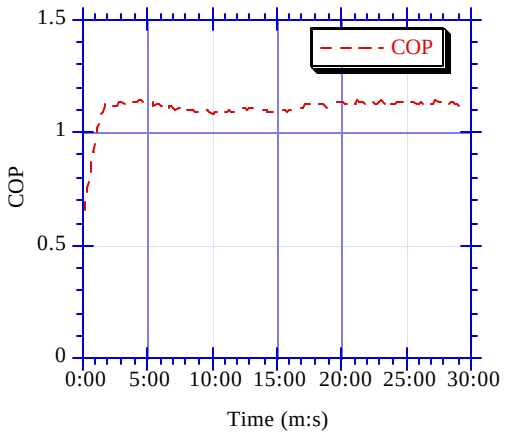

Figure 5.11 COP for 60 °F ambient case

5.6 Conclusions

In both of the cases analyzed in this chapter, the evaporator operated at a reduced capacity until the charge could be redistributed to its equilibrium location. Before cooling can begin, the temperature of the two-phase section of the evaporator must drop below the surrounding air temperature. When the evaporator contains little charge as a consequence of less off-cycle migration, or rapid emptying upon compressor startup, it can change temperature quickly. This allows the evaporator to begin cooling very early into the on-cycle. For the 60 °F case, it is believed that a similar amount of charge migrated to the evaporator during the off-cycle as for the 90 °F case. However, once the compressor started, the evaporator became immediately starved. This could be a consequence of the distribution of liquid refrigerant within the evaporator. As the refrigerant boiled during the off-cycle, it may have traveled through the evaporator tubing towards the exit. Once the compressor started, large slugs of liquid exited thereby starving the evaporator. This allowed the temperature of the remaining refrigerant to drop rapidly and begin absorbing heat from the freezer air. In contrast, a flooded evaporator needs more time to boil off some charge before its pressure and temperature can drop and heat transfer can begin. This is believed to cause the longer period of reduced evaporator capacity for the 90 °F ambient case. Since no boiling occurred during the off-cycle in that case, much of the refrigerant may have been trapped near the evaporator inlet, and fewer slugs of liquid were able to exit the evaporator. Thermodynamically, it is beneficial to remove the excess charge from the evaporator as quickly as possible, so that the quasi-steady evaporating temperature can be established, and full refrigerating capacity can be attained. However, this benefit is offset by the risk to compressor reliability.

Chapter 6: Capillary Tube/Suction Line Heat Exchanger

6.1 Introduction

Most modern refrigeration equipment uses a capillary tube/suction line heat exchanger to lower the refrigerant quality at the inlet to the evaporator, thereby increasing its capacity. The efficiency gains for an R-12 system are small (up to 5 percent increase in COP), however there are several other important benefits (Domanski *et al*, 1992). By heating refrigerant in the suction line, the heat exchanger ensures that only superheated vapor reaches the compressor, which helps prolong compressor life. It also heats the suction line above the ambient dew point temperature to prevent moisture from condensing on it. The price for these benefits is a loss in compressor efficiency as the suction temperature increases. For some refrigerants, such as R-22, the loss in compressor efficiency is greater than the gain in evaporator capacity, so suction line/capillary tube heat exchangers are not used. The heat exchanger also affects the mass flow rate through the capillary tube, which may impede charge redistribution during cyclic operation. This chapter will outline the transient behavior of the capillary tube, and consider the effects of the capillary tube/suction line heat exchanger on charge redistribution.

6.2 Effect of Condenser Subcooling on Charge Redistribution

During the off-cycle, most of the refrigerant in the system migrates to the cold evaporator, where it remains as a two-phase mixture (see Chapter 4). At the beginning of the on-cycle, depending upon the operating conditions, the compressor may draw liquid slugs from the evaporator (see Chapter 5). If too much charge is drawn from the evaporator, it becomes starved and is forced to operate with a high level of superheat at a reduced capacity.

The amount of superheat at the evaporator exit is not independent of other variables in the system. When the evaporator is superheated and its charge is low, the extra charge must be somewhere else in the system, such as in the condenser. The additional charge in the condenser can be seen as an increase in subcooling. The amount of condenser subcooling and evaporator superheat for a cycle in a 60 °F ambient room is plotted in Figure 6.1. The plot shows that in general, an increase in superheat is accompanied with an increase in subcooling.

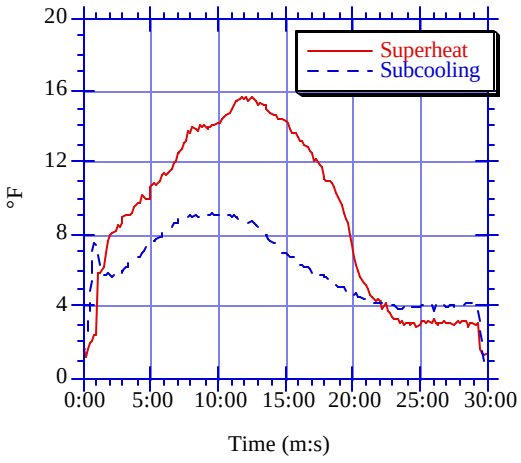

Figure 6.1 Superheat and subcooling during cycling

The effect on mass flow rate of varying degrees of condenser subcooling was analyzed using a finite difference computer simulation of the capillary tube/suction line heat exchanger (Peixoto, 1993). The simulation was run using inputs in accordance with experimental data. The evaporating pressure was set to 16 psia, and the condensing pressure to 113 psia. The condenser subcooling was varied from 0 to 7 °F, and the evaporator superheat was set at 5 °F. The results from this simulation are plotted in Figure 6.2. As expected, an increased level of subcooling increases the mass flow rate through the capillary tube. The refrigerant entering the capillary tube is slightly denser, and the flash point moves further up the tube. In this case, the mass flow rate increases by 0.33 lbs/hr for each additional degree of subcooling. By this mechanism, the system is able to allocate more charge to the evaporator when it needs it, thereby achieving a mass flow balance with the compressor. It is important to note that this effect ocurrs with or without the presence of a suction line/capillary tube heat exchanger. This is verified by running the simulation with an adiabatic capillary tube.

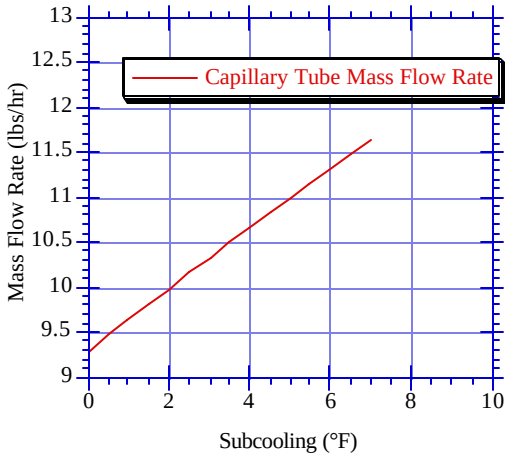

Figure 6.2 Effect of condenser subcooling on capillary tube mass flow rate

With certain evaporator/accumulator configurations, it is also possible that the compressor is unable to empty the evaporator at the start of the on-cycle. In this instance, the evaporator operates with a surplus of charge as the refrigerant slowly boils out. With excess charge in the evaporator, the condenser will have a low level of subcooling, or perhaps a saturated exit. This reduces the mass flow rate through the capillary tube, thereby aiding the charge redistribution. Again, this effect is independent of the presence of a capillary tube/suction line heat exchanger.

6.3 Effects of Suction Line/Capillary Tube Heat Exchanger on Charge Redistribution

The addition of a heat exchanger between the warm capillary tube and the cool suction line permits a higher mass flow rate through the capillary tube for a given inlet and outlet pressure. The capillary tube is sized with this in mind to fix a particular balance point with the compressor at a specific evaporating temperature. When not operating at this optimum condition, the entire system must adjust, resulting in a lower efficiency.

When the evaporator is starved, as it may be in the beginning of the on-cycle, it operates with a high level of superheat. The resulting suction line temperature is higher than if the evaporator was flooded, which lowers the

heat transfer from the capillary tube and moves the flashing point upstream. This reduces the mass flow rate through the capillary tube into the evaporator, thus it takes longer for the charge to redistribute and reduce the level of superheat.

The effect on mass flow rate of varying degrees of evaporator superheat was also analyzed using the finite difference computer simulation of the capillary tube/suction line heat exchanger (Peixoto, 1993). Again the simulation was run using an evaporating pressure of 16 psia, and a condensing pressure of 113 psia. This time the condenser subcooling was set at 5 °F, and the evaporator superheat was varied from 0 to 15 °F. The results from this simulation are plotted in Figure 6.3.

As expected, the maximum mass flow rate through the capillary tube for the specified evaporating and condensing pressures occurs with the minimum level of evaporator superheat, which corresponds to the coldest possible suction line. With 15 °F of superheat, the mass flow rate drops from 11.2 to 10.5 lbs/hr. This corresponds to a 0.05 lb/hr decrease in mass flow rate for each additional degree of superheat.

During the on-cycle of a refrigerator operating in 60 °F ambient room, a 22 minute period was observed during which the evaporator had on average 10 °F of superheat above its quasi-steady value at the end of the on-cycle (see Figure 5.8). Assuming that about 0.5 ounces of charge redistributed to reduce the level of superheating, the average difference in mass flow rates at the evaporator inlet and exit was 0.085 lb/hr. Using the simulation results, 10 °F of superheat reduced the capillary tube mass flow rate by 0.5 lbs/hr. Thus, without the capillary tube/suction line heat exchanger, the average difference in mass flow rates into and out of the evaporator would have been 0.585 lbs/hr. At this rate, the 0.5 ounces of charge could have been redistributed in as fast as 3.2 minutes. Clearly, the capillary tube/suction line heat exchanger reduces the flow rate into the evaporator when it needs more charge.

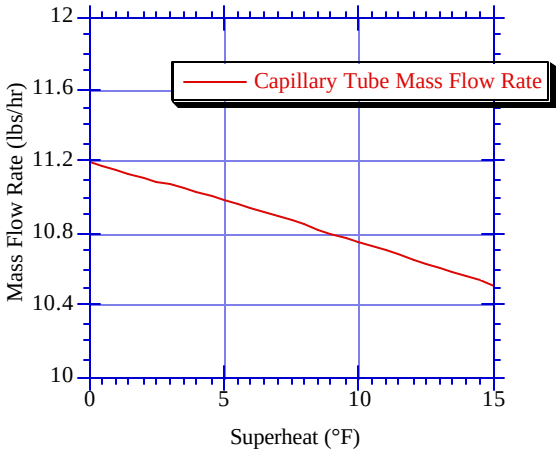

Figure 6.3 Effect of evaporator superheat on capillary tube mass flow rate

Conversely, when the evaporator contains a surplus of charge it operates with a lower quality exit than its steady state value. The two-phase section of the suction line lengthens, resulting in more heat exchange with the capillary tube. The additional heat transfer increases the capillary tube mass flow rate, which brings more charge into the evaporator when it already has too much. Thus, the suction line/capillary tube heat exchanger impedes charge redistribution in both cases, whether the evaporator is over- or under-charged.

6.4 Conclusions

The presence of the capillary tube/suction line heat exchanger slows the redistribution of charge to the evaporator when it has too much or too little charge. The negative effect of slower charge redistribution is most likely offset by the steady state efficiency gains that the heat exchanger provides. When the non-thermodynamic effects of the heat exchanger are considered, such as the protection it gives the compressor, it becomes clear that its use is warranted in refrigeration systems.

Chapter 7: Conclusions and Recommendations

7.1 Introduction

In the introduction of this report, two main goals were stated. The first is to identify and quantify the individual phenomena which degrade cycling performance. In the preceding six chapters, we have analyzed several of these factors, and they will be summarized here. The second goal is to determine which transients could be modeled using simple corrections to a quasi-steady model, and which would require a full transient simulation. This has not been specifically addressed in the previous chapters, so it will be discussed in this final chapter.

7.2 Thermal Mass Effects

Since it stored heat during the on-cycle, and rejected it during the off-cycle, the compressor shell temperature was lower throughout the on-cycle. It appears that the shell temperature may influence the isentropic efficiency of the compressor; however our data is inadequate to quantify this effect. Additional experiments are being designed to test this. The clearly beneficial effect of the lower shell temperature, a reduction in the compressor discharge temperature, was found to have minimal effect on the condenser for cases when its exit was subcooled. This effect is likely to reduce the condensing temperature in cases with a saturated condenser exit, however our data sets do not include any cycling points with a saturated condenser exit to verify this.

The thermal mass of the heat exchangers in the experimental refrigerator were found to have a negligible impact on performance, thus from this standpoint, no changes from a steady state model would be required. However, if the heat exchangers were very massive, they could continue to transfer heat during the off-cycle. This would lower the average temperature difference with between the heat exchangers and their surrounding air, which would reduce irreversibilities. A simulation of this effect would require a set of differential equations to model the transient conduction.

The thermal mass of the cabinet is unimportant from a design standpoint. It will not affect the percent run time or the COP of the refrigerator; however, a heavier cabinet will reduce the cycling frequency. It was shown in Chapter 2 that the cabinet could be modeled using a simple lumped capacitance equation. The overall conductance of the cabinet was found to be a function of the air flow patterns inside the compartments. During the off-cycle, with the evaporator fan off, the conductance of the freezer compartment may drop as much as 20 percent, and the conductance of the refrigerator compartment by as much as 10 percent. This is an important consideration whether using a quasi-steady or a full transient model.

7.3 Refrigerant Dynamics

One shortcoming of quasi-steady models is that they do not take into account refrigerant dynamics. During cycling, the refrigerant charge moves between various components in the system as it tries to maintain a balance point. Because of the maldistribution of charge, some cycling points cannot be modeled as quasi-steady.

During the off-cycle, up to 5.5 ounces of refrigerant migrate through the capillary tube into the evaporator, bringing with it 15 to 30 Btu of energy. The migration process can be split into two distinct modes: liquid migration, which occurs during the beginning portion of the off-cycle, and vapor migration, which accounts for the remainder of the migration process. The relative amounts of liquid and vapor migration, which are primarily determined by the

condenser geometry, affect how much energy (between 15 and 30 Btu) was brought into the evaporator during the off-cycle. The liquid migration mass flow rate can be modeled using an adiabatic capillary tube model, and vapor migration behaves like Fanno flow. The main difficulty in modeling the migration process is in determining how much liquid migrates before vapor migration takes over.

In some instances, such as when the condensing temperature is high, the migrating refrigerant raises the temperature of the evaporator above the freezer air temperature. In this case, most of the 15 to 30 Btu are transferred to the freezer air, which degrades efficiency. However, when the migrating refrigerant is cool, such as when the condensing temperature is low, the evaporator temperature remains below the freezer air temperature for the duration of the off-cycle. This results in heat transfer from the air to the refrigerant inside the evaporator. In this case, the 15 to 30 Btu remain in the evaporator and are never transferred to the freezer air, so no loss in efficiency occurs as a direct result of the migration. The heat transfer from the air for one particular data set was estimated to be only 2 Btu, hence the refrigerating effect is most likely negligible. However, the heat transfer begins to boil the migrated refrigerant, which affects the distribution of liquid and vapor within the evaporator. This can affect the redistribution of charge during the subsequent on-cycle.

At the beginning of the on-cycle, most of the charge that migrated to the evaporator must be removed before quasi-steady operation can be achieved. Thermodynamically it is best to remove the excess charge as quickly as possible, so that the evaporating temperature can drop, and heat transfer between the evaporator and the freezer air can begin. For the data sets used in this analysis, the initial phase of the redistribution process took between 2 and 4 minutes, during which the evaporator heat transfer rate was greatly reduced. This was found to be a major contributor to cycling losses; the COP during these first minutes rose linearly from 0 nearly up to its maximum value. The effect on overall COP therefore depends on cycle length and the amount of time it takes to redistribute the excess charge at the beginning of the cycle.

The speed of the redistribution process depends primarily on whether refrigerant exits the evaporator as liquid or vapor. If the excess charge vaporizes before leaving the evaporator, an additional 21 Btu could be absorbed by the refrigerant from the freezer air. However, the redistribution process would be slower, thus prolonging the period of reduced evaporator capacity. From this standpoint, slugging the liquid out of the evaporator is preferable, except that it may damage the compressor. Perhaps an accumulator could be added at the compressor inlet, or the compressor shell itself could be designed to act as an accumulator, to prevent damage from liquid slugs.

If too much charge is pulled out of the evaporator at the beginning of the on-cycle, the system will operate with a high level of superheat at a reduced capacity. While this affects COP, it appears to be thermodynamically preferable to the effect of refrigerant maldistribution during the first few minutes of the on-cycle.

For systems with a low-side oil sump, such as those with reciprocating compressors, up to 0.4 ounces of refrigerant dissolve into the oil during the off-cycle, and boil out during the on-cycle. This effect is reversed and much more pronounced for high-side oil sump systems, such as those with rotary compressors. In this case, up to 6 ounces of refrigerant may dissolve into the oil during the on-cycle, and boil out during the off-cycle.

By absorbing some of the extra charge from the evaporator during the off-cycle, a compressor with a low-side sump allows the evaporator to return to its optimum charge level earlier in the on-cycle. However, this might not

affect the rate of decrease in low-side pressure and the rate of increase in evaporator capacity. As the refrigerant boils out of the oil, it tends to increase the low-side pressure, thus prolonging the period of lower evaporator capacity.

In a high-side sump system, much more charge is available to migrate through the capillary tube into the evaporator during the off-cycle. In addition to the refrigerant in the condenser, the refrigerant dissolved in the oil (up to 6 ounces) can migrate as well. With roughly twice the charge in the evaporator by the end of the off-cycle, it is unlikely that the evaporator could become starved at the beginning of the on-cycle. However, as the compressor begins depleting the evaporator, some of the refrigerant gets absorbed by the oil, thus the compressor collects charge. This lowers the mass flow rate into the condenser, hence the mass flow rate into the evaporator is also lower. In this manner, the high-side oil sump speeds the removal of charge from the evaporator. Future experiments are being designed to quantify these effects.

The redistribution of refrigerant during the on-cycle substantially affects refrigerator performance. Unfortunately it is complex to model, primarily because it is difficult to predict how much of the extra charge slugs out of the evaporator as liquid, and how much of it leaves as vapor. This makes it difficult to predict the redistribution time, and whether or not the evaporator will become starved. For this reason, the beginning few minutes of an on-cycle cannot be modeled using a quasi-steady simulation. It would be extremely difficult to make a simple correction to a steady state model, since the loss in evaporator capacity depends on so many variables.

The addition of a check valve to prevent off-cycle migration may eliminate some cycling losses. However, the evaporator would be even more likely to become starved upon startup, since it would contain much less charge at the end of the off-cycle. This would still result in a loss in COP until the evaporator could return to its steady-state charge level.

7.4 Capillary Tube/Suction Line Heat Exchanger

Although the presence of an interchanger can improve the steady state COP by as much as 5 percent, it can degrade cycling performance by prolonging charge maldistribution. In one observed case, the evaporator operated for 22 minutes (66 percent of the on cycle) with an excessive level of superheat, resulting in an average 2 percent reduction in COP. Each additional one degree Fahrenheit of superheat at the suction line inlet was found to reduce the mass flow rate in the capillary tube by 0.05 lbs/hr. Without the interchanger present, it is estimated that the additional charge required by the evaporator could have been distributed in 3 minutes instead of 22. It should be a simple matter to model the interchanger using quasi-steady relations for the mass flow rate and heat transfer, except during the sharp transients at the very beginning of the on- and off-cycles.

7.5 Instrumentation and Data Acquisition

For a proper analysis, it is extremely important to have accurate instrumentation. The pressure and power transducers should be recalibrated before each use, and their drift should be monitored throughout data acquisition. The current data sets indicate typical pressures at various points in the system during both steady state and cycling cases. This information should be used when choosing pressure transducers for the next experimental refrigerators. Transducer accuracy is usually a function of measurement range, thus the smallest allowable range should always be chosen. The same applies for power transducers. Before installation in the refrigerator, all thermocouples should be

calibrated using a temperature reference. The calibration of the thermocouple terminal panels in the data acquisition system should be checked periodically for temperature drift.

This work has shown that microphones may be a valuable tool for analyzing refrigerant movement during cycling. It is important to use high quality recording equipment to minimize extraneous noise generation. Analog or digital filters could be developed to remove fan and compressor noise, which dominate the recordings. Every attempt should be made to reduce the effects on refrigerator performance introduced by the instrumentation. This includes minimizing thermal mass, added volume, and extra insulation which may occur as a result of mounting instrumentation devices.

For future projects, it is recommended that cycling data be taken before steady state data. This way, the cycling data can be examined first, and relevant steady state points can be determined beforehand. It is also important to take a complete set of both cycling and steady state data before making any changes to the system which could affect performance. The data should be taken as quickly as possible to minimize the effects of the inevitable minor leaks that seem to accompany every instrumented refrigerator.

In order to maximize the number of data points for which mass flow meter was operable, much of this analysis was done using an overcharged refrigerator. This will be less important in the future because the current mass flow data have been used to adjust and improve the compressor map (Admiraal, 1993). Additional experiments should be conducted with an optimally charged refrigerator to observe any differences.

References

Admiraal, D.M., and Bullard, C.W., *Variable Conductance Models of Refrigerator/Freezer Heat Exchangers*, Forthcoming, Air Conditioning and Refrigeration Center, University of Illinois at Urbana-Champaign, 1993.

American Society of Heating, Refrigerating and Air-Conditioning Engineers, Inc., *1989 ASHRAE Handbook Fundamentals*, ASHRAE, Atlanta, 1989.

Arthur D. Little, Inc., *EPA Refrigerator Analysis Program User's Manual Peer Draft*, 1992.

Cavallaro, A., University of Illinois at Urbana-Champaign, personal communication, 1993.

Dabiri, A.E., and Rice, C.K., "A Compressor Simulation Model With Corrections For the Level of Suction Gas Superheat," *ASHRAE Transactions*, Vol. 87, Part 2, pp. 771-782, 1981.

Domanski, P.A., Didion, D.A., and Doyle, J.P., "Evaluation of Suction Line - Liquid Line Heat Exchange in the Refrigeration Cycle," *Procedings of the IIR-Purdue Refrigeration Conference*, pp. 131-139, 1992.

Grebner, J.J., and Crawford, R.R., *The Effects of Oil on the Thermodynamic Properties of Dichlorodifluoromethane (R12) and Tetrafluoroethane (R-134a)*, ACRC TR-13, Air Conditioning and Refrigeration Center, University of Illinois at Urbana-Champaign, 1992.

Incropera, F.P., and DeWitt, D.P., *Fundamentals of Heat and Mass Transfer*, 2nd ed., John Wiley & Sons, New York, 1985.

Janssen, M.J.P., deWit, J.A., and Kuijpers L.J.M., "Cycling Losses in Domestic Appliances: An Experimental and Theoretical Analysis," *International Journal of Refrigeration*, Vol. 15, No. 3, pp. 152-158, 1992.

Melo, C., Da Silva Ferreira, R.T., Horn Pereira, R., and Ribeiro Negrao, C.O., "Dynamic Behaviour of a Vapor Compression Refrigerator: a Theoretical and Experimental Analysis," *Status of CFCs - Refrigeration Systems and Refrigerant Properties*, Proceedings of the International Institute of Refrigeration, pp. 141-149, 1988.

Moran, M.J., and Shapiro, H.N., *Fundamentals of Engineering Thermodynamics*, 1st ed., John Wiley & Sons, New York, 1988.

Mulroy, W.J., and Didion, D.A., "Refrigerant Migration in a Split-Unit Air Conditioner," *ASHRAE Transactions*, Vol. 91, Part 1A, pp. 193-206, 1985.

Omega Engineering, Inc., *The Temperature Handbook*, Vol. 27, 1989.

Pedersen, C.O., Professor of Mechanical Engineering, University of Illinois at Urbana-Champaign, personal communication, 1992.

Peixoto, R., *Modeling of Refrigerant Flow Through Capillary Tubes*, Forthcoming, Air Conditioning and Refrigeration Center, University of Illinois at Urbana-Champaign, 1993.

Porter, K.J., and Bullard, C.W., *Modeling and Sensitivity Analysis of a Refrigerator/Freezer System*, ACRC TR-31, Air Conditioning and Refrigeration Center, University of Illinois at Urbana-Champaign, 1992.

Reeves, R.N., Bullard, C.W., and Crawford, R.R., *Modeling and Experimental Parameter Estimation of a Refrigerator/Freezer System*, ACRC TR-9, Air Conditioning and Refrigeration Center, University of Illinois at Urbana-Champaign, 1992.

Sanvordenker, K., Techumseh Products Company, personal communication, 1992.

Staley, D.M., Bullard, C.W., and Crawford, R.R., *Steady State Performance of a Domestic Refrigerator Using R12 and R134a*, ACRC TR-22, Air Conditioning and Refrigeration Center, University of Illinois at Urbana-Champaign, 1992.

Stoecker, W.F., and Jones, J.W., *Refrigeration and Air Conditioning*, 2nd ed., McGraw Hill, New York, 1982.

Stoecker, W.F., *Design of Thermal Systems*, 3rd ed., McGraw Hill, New York, 1989.

Sugalski, A., Jung, D., and Radermacher, R., "Quasi-Transient Simulation of Domestic Refrigerators," *Proceedings of the XVIII International Congress of Refrigeration*, Vol. III, pp. 1244-1249, 1991.

Wang, J., and Wu, Y., "Start-up and Shut-down Operation in a Reciprocating Compressor Refrigeration System with Capillary Tubes," *International Journal of Refrigeration*, Vol. 13, pp. 187-190, 1990.

Appendix A: Instrumentation

A.1 Data Acquisition System

An existing computer based data acquisition system, manufactured by Strawberry Tree Incorporated, was upgraded to gather data for this project. It was previously capable of monitoring up to 32 thermocouples and 24 voltage signal transducers, such as pressure or power transducers, simultaneously. Additional hardware was added to accommodate up to 48 thermocouples. The thermocouples are connected directly to model T21 terminal panels which are connected to model ACM2-16-16 data acquisition boards. Pressure transducers, power transducers, and the mass flow meter are connected to model T51 terminal panels, which are connected to either ACM2-12-16 or ACM2-12-8A data acquisition boards. These boards are mounted in a Macintosh IIx computer, which runs a software package called Workbench. The data acquisition computer was moved to cleaner area outside of the laboratory, and cables were extended between the terminal panels and the data acquisition boards. System accuracy is presented in Table A.1, and a block diagram is shown in Figure A.1.

Table A.1 Accuracy of data acquisition system

Measurement	Accuracy	Source
Thermocouple	±1.3°F (±0.7°C)	Manufacturer's literature
Thermocouple	± 0.73 °F (±0.41°C)	Staley, 1992
Thermocouple	± 0.53 °F (±0.29 °C)	Using tare values
Voltage	±0.2 V	Manufacturer's literature

Staley (1992) estimated the accuracy of the original setup experimentally, using Equation A.1. The precision error was determined to be ±0.53 °F and the bias is supplied by the manufacturer as 0.5°F. In an attempt to further reduce the uncertainties in temperature measurement, a tare system was implemented on recent data sets. After all of the thermocouples have soaked in an isothermal chamber for 48 hours, one is chosen as reference, in this case the chamber air temperature, and the remaining thermocouple readings are adjusted to match the reference. These adjustments are called the tare values, and they are typically less than 0.5°F. This in agreement with manufacturer's bias specification. The point of the tare values is to eliminate the bias error, and hence lower the overall uncertainty. Tare values are taken before each set of tests at each chamber temperature, and they are found to be relatively constant. By eliminating the bias error, the overall uncertainty becomes the precision error, which is in this case ± 0.53 °F.

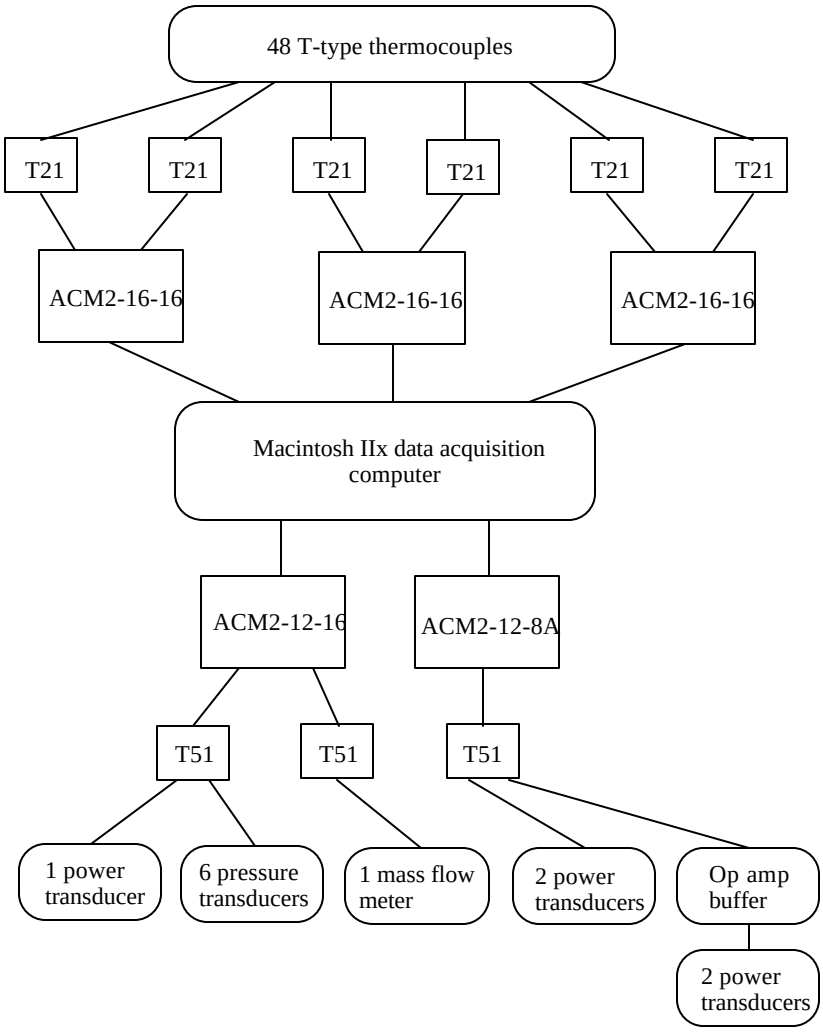

Figure A.1 Data acquisition system block diagram

$$\text{Uncertainty} = \sqrt{(\text{Bias})^2 + (\text{Precision error})^2} \qquad \text{A.1}$$

A.2 Refrigerant Temperatures and Pressure Taps

In earlier tests, refrigerant temperatures were measured using 0.0625 inch diameter stainless steel sheathed thermocouples (Omega type 304SST) mounted in brass instrumentation blocks as shown in Figure A.2 The brass blocks had threaded fittings which leaked frequently, and the entire block acted as a large thermal mass which may have dampened transients. The thermocouple sheaths presented a substantial pressure drop in the flow, and may have slowed the reaction of the junction to varying temperatures. The fittings added unnecessary volume to the system which may have affected the optimum charge of refrigerant. To reduce these shortcomings, the instrumentation blocks and the thermocouples were eliminated, and thinner 0.020 inch diameter thermocouples were mounted directly into the refrigerant lines as shown in Figure A.3.

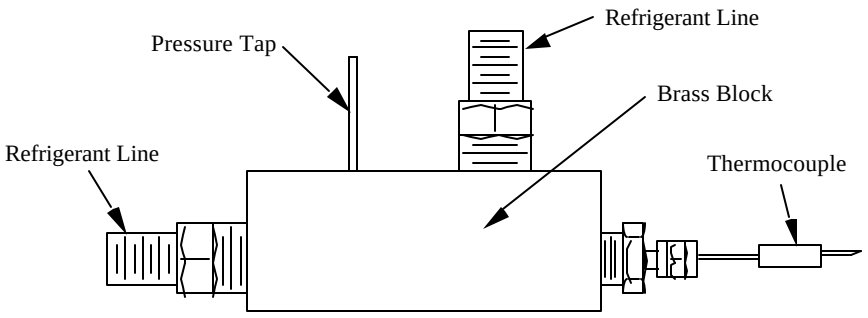

Figure A.2 Brass instrumentation block

An immersion thermocouple is typically placed in an existing copper elbow in the refrigerant line through a short guide tube. The guide tube is silver soldered to the elbow to provide support for the sheath. After the soldering is completed, a 0.020 inch diameter hole is drilled through the refrigerant line wall. The thermocouple sheath can then either be soft soldered or epoxied in place. Placing thermocouples in the evaporator is complicated because of the difficulty in soldering to aluminum. Fortunately the tube wall is thick enough here to support the thermocouple. The aluminum is prepared by roughening the surface with sandpaper and then cleaning it with acetone. The thermocouple sheath is epoxied in place, and then taped along the adjoining evaporator tubing to provide additional support. No leaks have been detected in these arrangements, and the soft soldering has had no known ill effects on thermocouple performance.

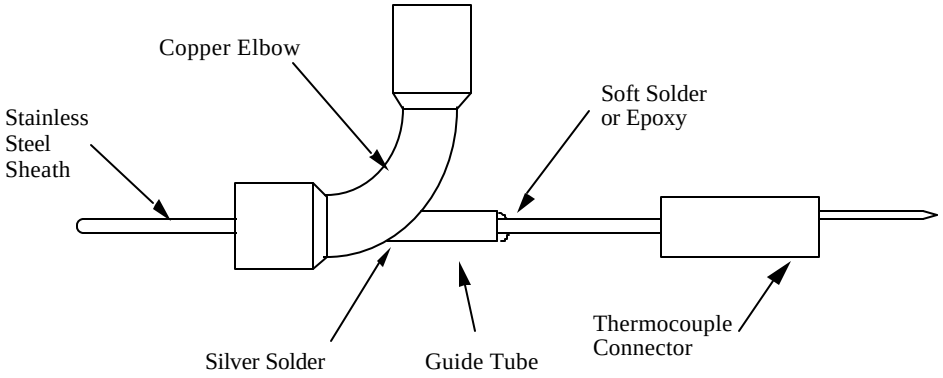

Figure A.3 New thermocouple instrumentation method

Pressure taps were added directly to the refrigerant lines, and supported with guide tubes as shown in Figure A.4. The guide tube is first silver soldered in place, and then a 1/16 inch hole is drilled through the refrigerant line. The pressure tap line is then soft soldered in place. This method minimizes added thermal mass and volume.

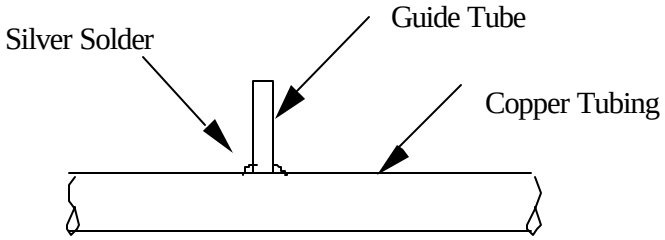

Figure A.4 New pressure tap instrumentation technique

A.3 Surface Thermocouples

In order to evaluate the performance and applicability of surface thermocouples, several were mounted adjacent to immersion thermocouples in the refrigerant lines, as shown in Figure A.5. In order to mount a surface thermocouple, the copper tube is roughened with sand paper, and then cleaned with acetone. A T-type thermocouple is wrapped several times around the tubing and secured in place with a thread. This provides strength and also minimizes heat conduction through the thermocouple wire. It is important to maintain good contact between the thermocouple junction and the copper tubing. A drop of thermally conducting epoxy (Wakefield Engineering part number 152-1-A) is placed over the junction. After allowing sufficient drying time, a 3.0 inch wide strip of 0.5 inch thick adhesive-backed foam insulation is wrapped around the assembly to ensure that no fin effect occurs with the thermocouple wire.

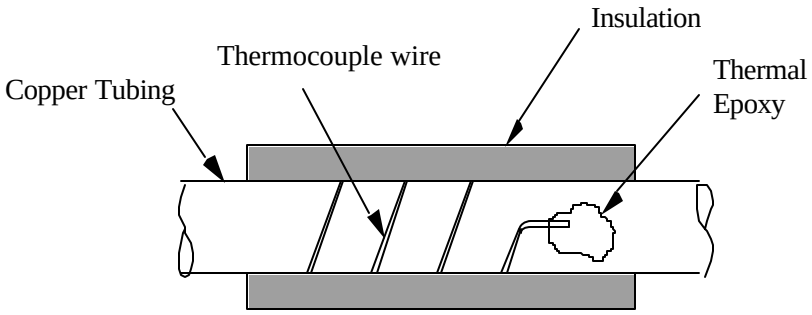

Figure A.5 Surface thermocouple

The goal is to determine if surface thermocouples agree well enough with immersion thermocouples to eliminate the need for immersion thermocouples on future projects. Surface thermocouples are easier to install because they do not penetrate the refrigerant line. This prevents pressure drops as well as potential leaks. During steady state operation the difference between surface and immersion temperatures for 40 data points is summarized in Figure A.6 and Table A.2.

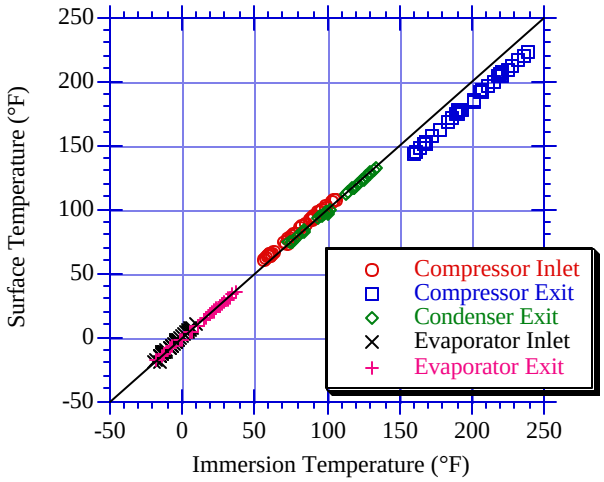

Figure A.6 Steady state comparison of surface and immersion thermocouples

A quick glance at Figure A.6 shows that most of the thermocouples agree quite well, with the exception of the pair at the compressor exit. Here the surrounding air averages about 100 °F cooler than the refrigerant temperature. This would tend to cool the surface, and lower the thermocouple's temperature. Secondly, the refrigerant exiting the compressor is in the vapor phase which does not transfer heat to the tubing as well as a liquid would. These are probably the major factors contributing to the large temperature difference. The surface thermocouple itself is not suspected to cause the large error because it agrees perfectly with the immersion thermocouple when the refrigerator is turned off and at thermal equilibrium with its surroundings. Another possible explanation is that the thermocouple is mounted improperly, but there are no visual indications of this.

Table A.2 Steady state comparison of surface and immersion thermocouples

Location	Refrigerant Phase	Air - Immersion [°F]		Surface - Immersion [°F]	
		RMS	Standard Deviation	RMS	Standard Deviation
Compressor Inlet	vapor	16.2	3.8	1.8	0.8
Compressor Exit	vapor	98.2	8.6	15.4	1.2
Condenser Exit	2-phase, liquid	8.5	3.5	1.3	0.7
Evaporator Inlet	2-phase	17.1	10.1	0.9	0.9
Evaporator Exit	2-phase, vapor	6.9	6.78	1.3	0.9

The other four surface thermocouples are in better agreement with their immersion counterparts. The difference between these surface and immersion temperatures is relatively small, and a correlation can be created between them. In future projects, immersion thermocouples could be eliminated in favor of surface thermocouples using these correlations. It is possible that the performance of these surface thermocouples may be improved by more insulation, although too much insulation could begin to affect system performance.

A surface thermocouple can be crudely modeled as shown in Figure A.7, which contains a simplified resistive network representation. The thermal resistivity of the metal tubing is very small, thus the tube is assumed to be isothermal. Under this assumption, the insulation has little effect on the surface temperature. Axial conduction through the tube would make the wall temperature the same under the insulation as it is adjacent to it. With these simplifications, the one-dimensional heat transfer is characterized by Equation A.2

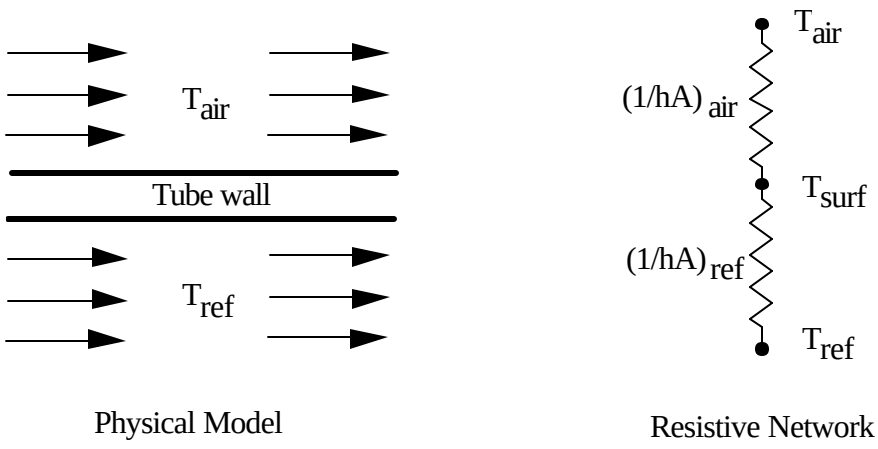

Figure A.7 Surface thermocouple model

$$\frac{(T_{air} - T_{surf})}{(1/hA)_{air}} = \frac{(T_{surf} - T_{ref})}{(1/hA)_{ref}} \quad \text{A.2}$$

Rearranging and grouping the heat transfer coefficients as a single parameter, k, yields Equation A.3.

$$(T_{air} - T_{surf})k = (T_{surf} - T_{ref}) \quad \text{A.3}$$

The temperature of the refrigerant can then be estimated using Equation A.4.

$$T_{ref} = T_{surf} - k(T_{air} - T_{surf}) \quad \text{A.4}$$

Assuming that k does not vary substantially for different refrigerator operating conditions, a least squares curve fit is made for the data set. At locations where the flow may sometimes be single phase and other times 2-phase, different k values are obtained for each condition. The k values are summarized in Table A.3, and predicted versus measured refrigerant temperatures are plotted in Figures A.8 and A.9 for the compressor exit and the evaporator exit. The other thermocouples yield similar results.

Table A.3 Surface thermocouple k values

Location	Refrigerant Phase	Tube Material	k	RMS Error (°F)	Standard Deviation
Compressor Inlet	vapor	copper	0.127	0.59	0.59
Compressor Exit	vapor	copper	0.177	2.51	2.53
Condenser Exit	2-phase	copper	0.138	0.63	0.63
Condenser Exit	subcooled	copper	0.267		
Evaporator Inlet	2-phase	aluminum	0.035	0.71	0.70
Evaporator Exit	2-phase	aluminum	0.000	0.34	0.29
Evaporator Exit	vapor	aluminum	0.259		

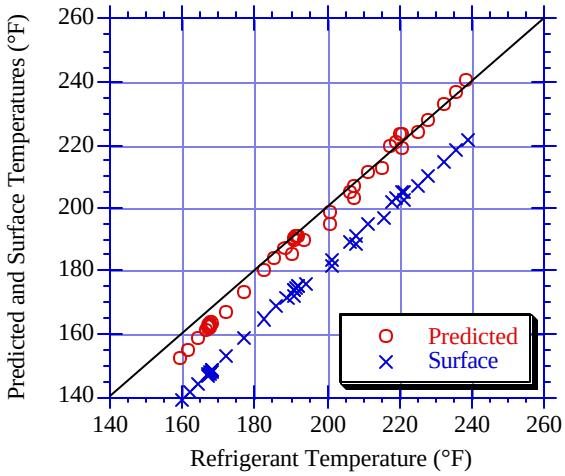

Figure A.8 Surface thermocouple correlation at compressor exit

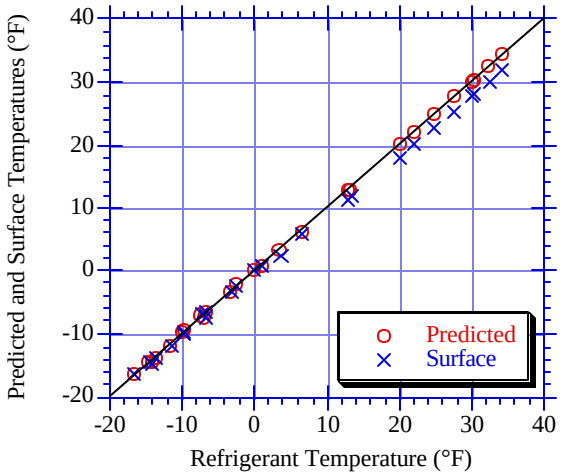

Figure A.9 Surface thermocouple correlation at evaporator exit

The correlations work very well in all locations, with the possible exception of the compressor exit, where the root mean square error is 2.51 °F. The simple resistive network representation may not work well here because the difference between refrigerant and air temperatures is nearly 100°F. This large temperature difference amplifies the importance of an accurate k value. Also, the insulation could be substantially affecting the tube wall temperature which would invalidate the one-dimensional heat transfer assumption. Finally, the k value is really a function of refrigerant and air flow rates. While the air flow rate is relatively constant throughout the data set, the refrigerant mass flow rate may vary by a factor of 2. It is not yet known if the k values would work well on another installation, however a second refrigerator has been equipped with surface thermocouples and it is recommended to repeat this analysis on that unit.

The surface thermocouples were also evaluated using a transient data set taken at an ambient temperature of 75°F. Here they do not work nearly as well. Figures A.10 and A.11 compare a subset of the transient data at the

compressor exit and evaporator inlet, and Table A.4 summarizes the maximum and RMS errors for the complete data set for all five sets of thermocouples. The maximum errors occur during sharp transients and are not representative of typical errors, which are listed in the RMS error column. This indicates that the surface thermocouples may be most useful when analyzing quasi-steady state operation, such as at the end of on or off cycles.

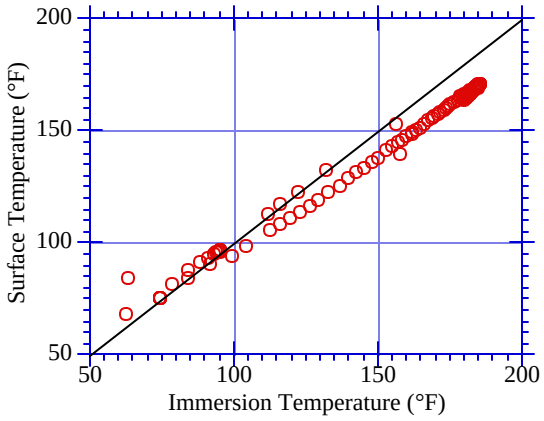

Figure A.10 Transient comparison of surface and immersion thermocouples at compressor exit

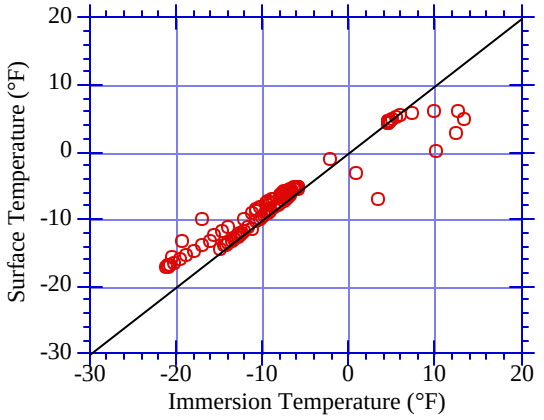

Figure A.11 Transient comparison of surface and immersion thermocouples at evaporator inlet

Table A. Comparison of surface and immersion thermocouples during cycling

Location	Surface - Immersion Temperature [°F]		
	Maximum Difference	RMS	Standard Deviation
Compressor Exit	28.5	7.2	6.5
Compressor Inlet	32.7	3.2	3.2
Condenser Exit	10.2	1.1	1.1
Evaporator Inlet	52.1	4.0	3.8
Evaporator Exit	11.9	1.3	1.1

The surface thermocouples tend to lag behind the immersion ones, as shown in Figure A.12 for the compressor exit and Figure A.13 for the evaporator inlet. Because the rate of change of temperature in the refrigerant during cycling is not constant, the lag is not constant either. One explanation for this is that it takes a finite amount of time for heat to conduct through the tube wall, hence the surface temperature lags behind the refrigerant temperature. The correlation developed for steady state can be applied to transient data with moderate success as shown in Figures A.14 and A.15 for the compressor exit and evaporator inlet respectively. Table A.5 summarizes the maximum and RMS errors using the correlations for all of the thermocouples.

One problem that arises in using the thermocouple correlations for transient data is that phase conditions might occur that do not exist for steady state. For example, during the initial startup, the condenser exit may be superheated, and this is clearly unrealistic for steady-state conditions. No k value has been estimated to describe this condition.

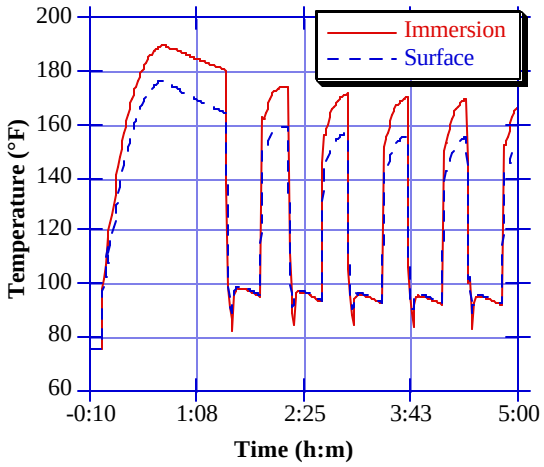

Figure A.12 Surface and immersion temperatures at compressor exit during cycling

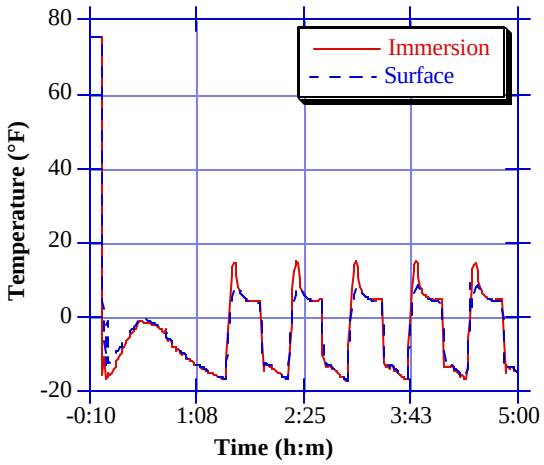

Figure A.13 Surface and immersion temperatures at evaporator inlet during cycling

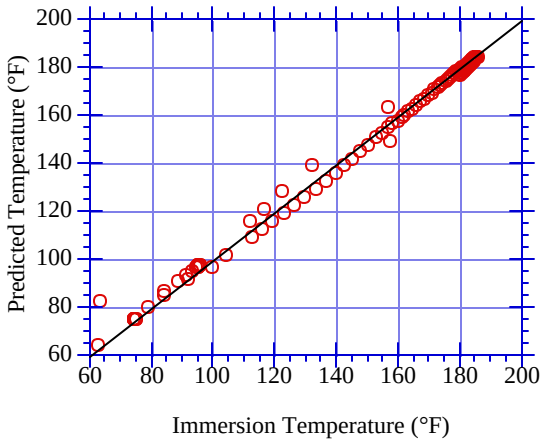

Figure A.14 Comparison of Predicted and measured refrigerant temperatures at compressor exit

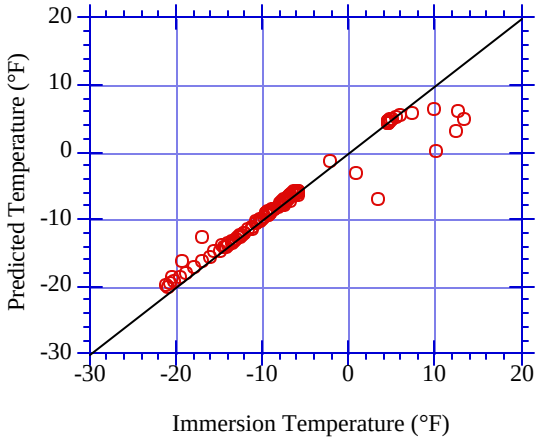

Figure A.15 Comparison of predicted and measured refrigerant temperatures at evaporator inlet

Table A.5 Surface thermocouple error summary for transient data

Location	Predicted - Immersion Temperature (°F)		
	Maximum	RMS	Standard Deviation
Compressor Exit	28.4	4.1	4.1
Compressor Inlet	30.9	3.8	3.6
Condenser Exit	13.5	1.5	1.3
Evaporator Inlet	50.7	4.0	3.7
Evaporator Exit	46.7	2.0	2.0

In general, the thermocouple correlations give large errors during sharp transients such as at the beginning of the on and off cycles. Near the ends of the on and off cycles the temperatures are close enough to steady state so that the steady state correlations can be used with some success. Again the compressor exit surface thermocouple is the farthest from its corresponding immersion thermocouple, although the others are not much better. At this time,

surface thermocouples cannot be recommended to reliably measure temperatures in a transient system such as a cycling refrigerator, especially when analyzing the sharp transients at the endpoints of a cycle.

The simple thermocouple model was developed assuming steady state heat transfer. This could be one reason that the model does not work as well for transient operation. Perhaps a more complete model could be developed to include the thermal mass of the tube wall, however this added complexity might make the correlations impractical to use.

A.4 Power Transducers

Several types of power transducers, made by Ohio Semitronics and Scientific Columbus, are used to measure power input to electric motors and resistance heaters. Their model numbers and accuracies are listed in Table A.6. The transducers output either a voltage signal or a current signal, which is converted to a voltage signal through a precision resistor, to the data acquisition system. The voltage signal is measured and fed into a curve fit which provides the power in watts. The actual uncertainty in power measurement is the sum of the uncertainties of the transducer signal, the data acquisition system, and the curve fit.

Table A.6 Power transducer application and accuracy

Model	Application	Current (Amp)	Voltage (Volts)	Manufacturer accuracy	Measured accuracy
PC519E	System	0 - 15	0 - 150	±7.5W	±0.4W (0-15W) ±1.8W (15-230W) ±8.6W (230-313W)
PC519E	Cond Fan	0 - 15	0 - 150	±7.5W	
PC5103C	Evap Fan	0 - 1	85 - 135	±0.5W	
XL-5C5-A2	Freezer Heat	0 - 5	120	±1.25W	
XL-5C5-A2	Refrig. Heat	0 - 5	120	±1.25W	
Valhalla Scientific 2100	Accuracy Check	0 - 0.2	0 - 150	± 0.25% Reading ± 0.06W	
		0 - 2	0 - 300	± 0.25% Reading ± 0.6W	
		0 - 20	0 - 600	± 0.25% Reading ± 6W	

In order to see if the overall accuracy is substantially worse than the manufacturer's specifications, the PC519E power transducer was compared with a stand-alone power analyzer, a Valhalla Scientific model 2100. Its accuracy is also listed in Table A.6. Various combinations of fan motors and light bulbs were connected to both power transducers simultaneously. A comparison of the power measured by the PC519E through the data acquisition system to power displayed on the Valhalla Scientific 2100 is presented in Figure A.16. Overall the agreement is very good over the entire range. The largest discrepancies occurred when measuring powers over 230 W, perhaps because the accuracy of the Valhalla Scientific 2100 drops significantly at higher powers. The maximum absolute error was 2.9 W (1.1%), which occurred when measuring a 260W load. The maximum percentage errors occurred when measuring powers less than 20 W, in this case 2.7 % which corresponded to a 0.7 W difference.

The accuracy of the data acquisition system is bounded by the absolute difference between the two readings given by the measurement devices, plus the accuracy rating of the Valhalla Scientific 2100, assuming that the manufacturer's accuracy claims are legitimate. This information is summarized in Table A.6 also. The actual accuracy is most likely better than these worst case calculations. Since the Valhalla Scientific 2100 is only accurate to ±0.25% of the reading ± 6W when the current is over 2 A, the results of this comparison in the upper power range are not very meaningful. Additional testing should progress as soon as a more accurate reference power measurement device becomes available.

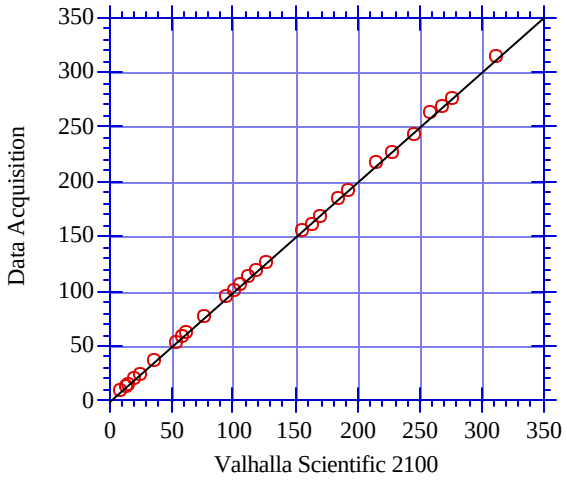

Figure A.16 Comparison of PC519E and Valhalla Scientific 2100 power transducers

Appendix B: Cabinet Heat Loads

Several methods for determining the overall heat transfer conductance of a domestic refrigerator cabinet have been implemented. All are based on a reverse heat leak test, however different air circulation and heating methods are used. The least intrusive and most realistic method is preferred, as long as it produces consistent results. A summary of the results is presented in Table B.1, and an explanation of the methods follows.

Table B.1 Summary of UA testing methods

Experimenter	Circulation	Data Points	UA_{frig} [W/°F]	UA_{frez} [W/°F]
Dean Staley	Sealed compartments 2 hair dryers	3	1.02	0.58
Ron Reeves	Sealed compartments 2 105cfm muffin fans	1	1.01	0.412
Dave Admiraal	Sealed compartments 2 105cfm muffin fans	3	1.035	0.433
Paul Rubas	Open compartments 1 105cfm muffin fan 45cfm Evaporator fan	5	1.011	0.493
Paul Rubas	Open compartments 1 15cfm muffin fan 45cfm Evaporator fan	5	0.907	0.509
Paul Rubas	Open compartments 1 15cfm muffin fan 45cfm Evaporator fan (2nd run)	5	0.898	0.530

The first UA estimates were calculated by D. Staley (1992) using hair dryers to heat and circulate the air inside the freezer and fresh food compartments. The hair dryer fans were wired to run continuously, while the heating element was cycled by a proportional controller. The vents connecting the freezer and fresh food compartments were taped shut to eliminate heat transfer due to migrating air. The cabinets were heated to identical temperatures above the ambient test chamber temperature in order to transfer heat from inside the cabinet to the surroundings. By measuring temperatures and heat inputs, Equations B.1 and B.2 were solved independently for UA_{frig} and UA_{frez}:

$$Q_{frig} = UA_{frig}(T_{frig}-T_{amb}) \qquad \text{B.1}$$

$$Q_{frez} = UA_{frez}(T_{frez}-T_{amb}) \qquad \text{B.2}$$

The equations were solved using three sets of time averaged temperature and power data. The air stream leaving the hair dryer is very directional, hence its orientation may bias the results. A possible source of measurement error is the un-filtered, fluctuating power supplied to the chamber and electronic equipment. This was corrected by the addition of a power conditioner in December of 1991.

The second UA estimates were calculated by R. Reeves (1992) in the fall of 1991 using 14W, 105cfm muffin fans in both compartments. These fans allowed lower cabinet temperatures since they required less power than the hair dryer motors. Orientation may be less important since the fans always blow upwards. Additional heat was

provided by nichrome wire heating elements strung across the fan inlets. This time, the heating elements were controlled by a variac. The test and data reduction procedures remained unchanged. The results from this method are markedly different in the freezer compartment, possibly due to the replacement of interior panels which were damaged during the summer of 1991. Other possible sources for the differences are the altered air currents, or the un-filtered, fluctuating power provided to the test equipment.

Reeves' fall UA estimates were verified by D. Admiraal (1993) in the winter of 1992 using a similar procedure. By this time the power conditioner had been added to the test equipment, and power measurements became more consistent. Admiraal used the same fans and heating elements as Reeves did for his second test, except he used proportional controllers to cycle the heating elements. The result for the refrigerator cabinet is similar to Reeves', however there is a slight difference in the freezer compartment. This may be caused by experimental error or different fan orientation.

The fan orientation was suspect in affecting the convection inside the compartments, hence a less intrusive UA test was desired. In order to better simulate the air flow patterns inside the compartments during normal operation, the evaporator fan was wired to run continuously and the muffin fan was removed from the freezer. The compartments are no longer isolated from each other; air is allowed to flow between them. The air temperatures from both compartments were carefully matched to minimize heat transfer from migrating air. New, larger heating elements were constructed to distribute heat more evenly throughout the cabinets. At first, the test was run with no fan in the refrigerator compartment; however, this resulted in a large temperature gradient. The 14W, 105cfm muffin fan was placed in the fresh food compartment to stir the air. It is placed on the wire rack as shown in Figure B.1. The inside of the refrigerator compartment is isothermal to ± 1.0 °F and in the freezer compartment ± 0.7 °F. A least squares minimization is implemented to simultaneously calculate UA_{frig}, UA_{frez}, and f_z, the evaporator fan air split fraction. The objective function is given in Equation B.3:

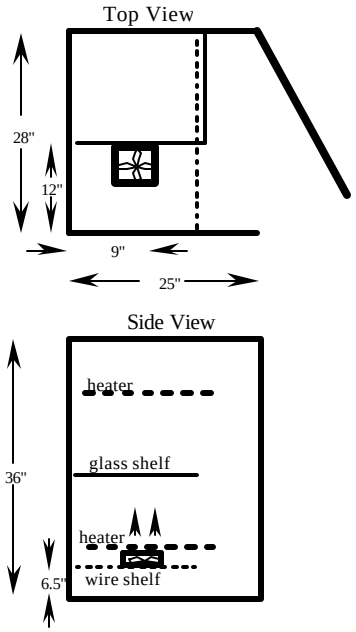

Figure B.1 Fan location

$$\text{Sigma} = (P_{evap} + Q_{frez} - UA_{frez}(T_{frez} - T_{amb}) + UA_{mullion}(T_{frig} - T_{frez})$$
$$+ (1 - f_z)(m)(c_p)(T_{fromfrig} - T_{tofrig}))^2$$
$$+ (Q_{frig} + (1 - f_z)(m)(c_p)(T_{tofrig} - T_{fromfrig})$$
$$- UA_{mullion}(T_{frig} - T_{frez}) - UA_{frig}(T_{frig} - T_{amb}))^2 \qquad \text{B.3}$$

where P_{evap} is the evaporator fan power, T_{tofrig} is the air stream temperature into the refrigerator compartment, and $T_{fromfrig}$ is the air stream temperature leaving the refrigerator compartment. This objective function is derived from an energy balance on the compartments as shown in Figures B.2 and B.3.

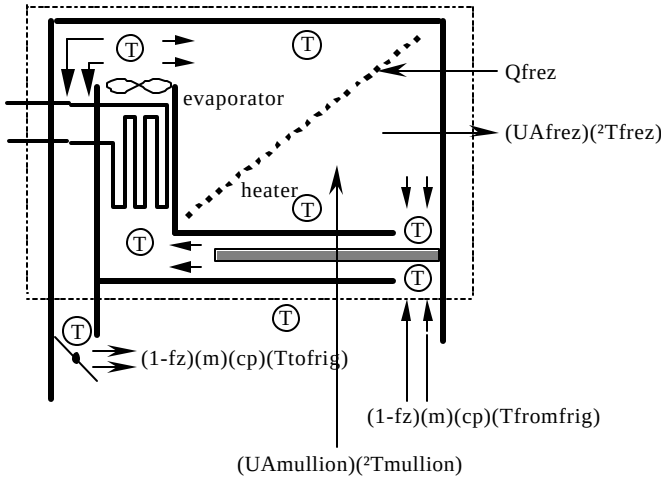

Figure B.2 Freezer Energy Balance

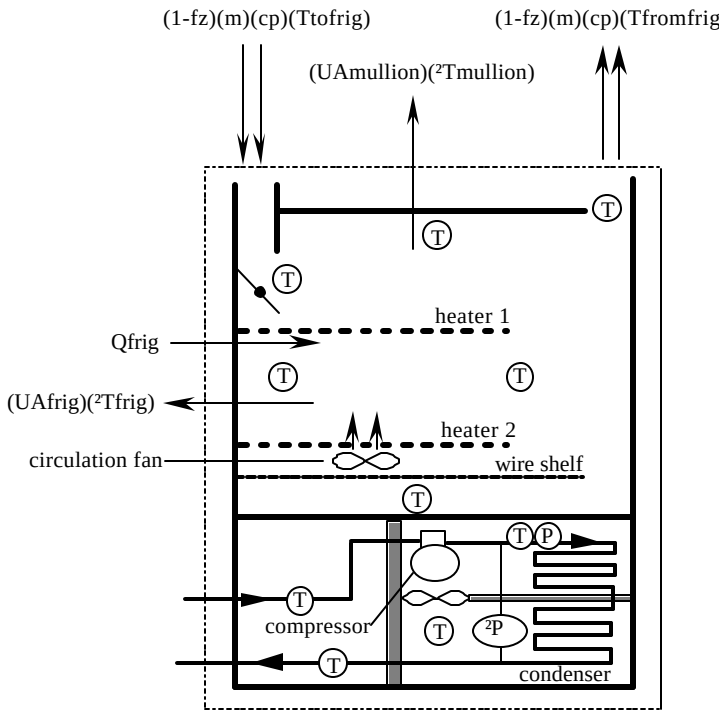

Figure B.3 Refrigerator Energy Balance

This parameter estimation results in a fairly steep minimum for the UA's as shown in Figure B.4. Although the UA values are firmly determined, the value for f_z is not. By setting f_z to different values and solving for the UA's, it becomes apparent that sigma is not a strong function of f_z. For this reason, f_z is set at 85% and only the UA's are estimated.

UA_{frez} is higher than the values obtained with muffin fans in sealed compartments. When the compartments were sealed, the space behind the evaporator contained stagnant air. This could act as an insulator and decrease cabinet conductance. Thus, when air is allowed to flow in this area, another heat transfer surface is introduced, thereby increasing cabinet conductance. In comparison with Staley's estimate, the evaporator fan may provide less convection than the hair dryer and hence the overall conductance is lower.

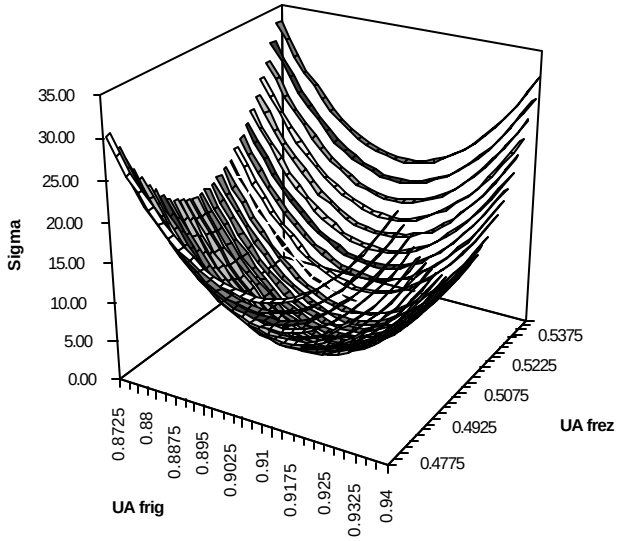

Figure B.4 Parameter estimation minimum

Q_{frez} is typically between 5 and 20W, and Q_{frig} is between 35 and 55W. According to manufacturer's specifications, the uncertainty on these measurements is less than +/- 0.25W. Thermocouple uncertainty is less than +/-0.9 °F, also according to manufacturer's specifications. The greatest uncertainties in the energy balance are $UA_{mullion}$ and the air split fraction, f_z. $UA_{mullion}$ was estimated by D. Admiraal (1993) to be 1.2 Watts/°F ±20%. This does not cause a large error since the mullion temperature difference, $\Delta T_{mullion}$, is very small and the resulting mullion term is on the order of 1W. The mass flow rate is calculated by multiplying the volumetric flow rate, v, with the air density at T_{tofrig}. The volumetric air flow rate was estimated by R. Reeves (1992) to be 45cfm. This is in agreement with the manufacturer's estimate of 44 to 46 cfm. The air split fraction was estimated to be 85% in the spring of 1991, and 70% in the fall of 1991. For this analysis, 85% is used. Because T_{tofrig} and $T_{fromfrig}$ are nearly equal, the heat transfer due to migrating air is typically from 2 to 5W, and thus the parameter uncertainties do not bias the results very much.

Finally, to test the hypothesis that convection is an important contributor to cabinet UA values, the large muffin fan was replaced by a 4W, 15cfm fan. This smaller fan is sufficient to keep the refrigerator compartment

isothermal to +/- 1.4 °F and the freezer to +/- 0.7 °F. The same objective function is used and again f_z is set at 85%. UA_{frez} is essentially unchanged, because nothing is changed in the freezer compartment. UA_{frig} decreases by about 10%. This can be explained by the lower convection coefficients which result from a smaller fan. UA_{frez} is probably more sensitive to fan selection because the compartment is much smaller.

Appendix C: Migration Model Program Listing

This appendix contains a True Basic™ program listing for the off-cycle migration model used in the Refrigerant Migration chapter. The generalized Newton-Raphson subroutine was provided by C.O. Pedersen (1992).

```
!LIQUID MIGRATION MODEL
!All temperatures in F
!All pressures in psia
!mass in lbs
!All properties for R12

OPEN #1: name"vapmig.out", CREATE NEWOLD
ERASE #1

DECLARE DEF DeDm
DECLARE DEF DeDT
DECLARE DEF Ecv
DECLARE DEF Psat
DECLARE DEF mflow
DECLARE DEF hliq
DECLARE DEF hvap
DECLARE DEF quality
DECLARE DEF vliq
DECLARE DEF vvap
DECLARE DEF DEevapDm
DECLARE DEF DEevapDt
DECLARE DEF vapormdot
DECLARE DEF SVapPres
DECLARE DEF Eevap

LET f = 0.03                    ! friction factor for cap tube
LET L = 125.5           ! length of cap tube in inches
LET D = 0.033           ! diameter of cap tube in inches
LET g = 1.091           ! gamma for R12 vapor
LET Pc = 171.2          ! initial condenser pressure
LET Pe = 18                     ! initial evaporator pressure
LET UAc = 1.65          ! Btu/hrR
LET UAe = 4.0           ! Btu/hrR
LET Tamb = 105          ! IN DEGREES F
LET Tc = 115.5          ! IN DEGREES F -> initial condenser temperature
LET Te = -14                    ! IN DEGREES F -> initial evaporator temperature
LET mc = 5.8/16         ! IN LBS -> the initial mass in the condenser
LET me = 1/16           ! IN LBS -> the initial mass in the evaporator
LET mc2 = 4.8/16        ! IN LBS -> mass in the condenser when vapor migration starts
LET Vc = 0.007666               ! Condenser volume IN FT^3
LET Ve = 45.704/1728    ! Evaporator volume in FT^3
LET deltat = 1/3600             ! time step is 1 second
LET migtime = 0         ! time into migration model in seconds
LET Qtot = 0                    ! starts total Q at zero
LET Tvap = 100          ! vapor temperature leaving the condenser is nearly constant
LET Tfrez = -4          ! initial freezer air temperature
LET ECum = 0

PRINT #1: "time";CHR$(9);"Tc";CHR$(9);"Pc";CHR$(9);"mass";CHR$(9);"mdot";CHR$(9);"Qevap"
PRINT "time";CHR$(9);"Tc";CHR$(9);"Pc";CHR$(9);"mass";CHR$(9);"mdot";CHR$(9);"Qevap"
```

```
LET Eevapinitial = Eevap(me, Te, Ve) !initial energy in evaporator in BTU

FOR counter = 1 to 2000

LET Pe = Psat(Te)
LET Pc = Psat(Tc)

LET xc = quality(mc, Tc, Vc)
IF xc >= 1 THEN
  !Superheated condenser condition
  LET xc = 1
  LET Pc = SVapPres(mc,Tc,Vc)
END IF

IF mc > mc2 THEN
!Liquid migration flow rate and enthalpy
  LET mdot = mflow(Pc) !flow rate in lb/hr
  LET h = hliq(102)
END IF

IF mc <= mc2 THEN
!Vapor migration flow rate and enthalpy
 LET mdot = -vapormdot(f, L, D, g, Pc, Pe,Tvap)*60/16   !flow rate in lb/hr
 LET h = hvap(Tvap)
 !Stoping condition
 IF mdot > -(0.1)*60/16 THEN              !checks if flow rate is miniscule
    PRINT "SIMULATION OVER"
    PRINT "Qtotal is ";Qtot;" BTU"
    LET Eadded = Eevap(me, Te, Ve) - Eevapinitial
    PRINT "Change In Evaporator Total Energy Is ";Eadded;" BTU"
    PRINT "Total energy added to freezer during migration is ";Eadded+Qtot;" BTU"
    PRINT "Total migration time is ";migtime/60;" minutes"
    PRINT "Ecum = ";ECum;" BTU"
    STOP
    CLOSE #1
    LET mdot = 0
 END IF
END IF

LET Qc = UAc*(Tamb - Tc)
LET Ect = DeDT(mc,Tc,Vc)
LET Ecm = DeDm(mc,Tc,Vc)
LET DTcDt = (Qc + mdot*h-Ecm*mdot)/Ect

LET Qe = UAe*(Te-Tfrez)
LET Eet = DEevapDt(me,Te,Ve)
LET Eem = DEevapDm(me,Te,Ve)
LET DTeDt = -(Qe + mdot*h - Eem*mdot)/Eet

!LET Qevap = -mdot*(DEevapDm(me,Te,Ve) - h)
LET Qtot = Qtot+Qe*deltat

LET migtime = migtime+3600*deltat
LET mc = mc + mdot*deltat
LET me = me - mdot*deltat
LET Tc = Tc + DTcDt*deltat
```

```
LET Te = Te + DTeDt*deltat
LET Tfrez = Tfrez + 0.01
LET ECum = Ecum - mdot*h*deltat
PRINT #1: migtime;CHR$(9);Tc;CHR$(9);Pc;CHR$(9);mc*16;CHR$(9);mdot*16/60;CHR$(9);Qe
PRINT migtime;CHR$(9);Tc;CHR$(9);Pc;CHR$(9);mc*16;CHR$(9);mdot*16/60;CHR$(9);Qe;CHR$(9);Te

NEXT counter

END             ! End of Main Program



!*********************************************************************
!                       FUNCTION SECTION
!*********************************************************************


!*********************************************************************
!                       ENERGY CALCULATION FUNCTIONS
!
FUNCTION Ecv(m, T, V)
!Total energy of the condenser in BTU
DECLARE DEF quality
DECLARE DEF uvap
DECLARE DEF uliq
LET mcp = 0.435 !BTU/R for condenser coils
LET x = quality(m,T,V)
IF x > 1 THEN LET x = 1
LET u = uliq(T) + x*(uvap(T) - uliq(T))
LET Ecv = mcp*(460+T) + m*u
END FUNCTION

FUNCTION Eevap(m, T, V)
!Total energy of the evaporator in BTU
DECLARE DEF quality
DECLARE DEF uvap
DECLARE DEF uliq
LET mcp = 2*0.72025    !BTU/R
LET x = quality(m,T,V)
LET u = uliq(T) + x*(uvap(T) - uliq(T))
LET Eevap = mcp*(460+T) + m*u
END FUNCTION

!*********************************************************************
!                       DERIVATIVE CALCULATION FUNCTIONS
!
FUNCTION DeDm(mass, Tc, Vol)
DECLARE DEF Ecv
LET deltam = 0.000625     !1/100 ounce
LET DeDm = (Ecv((mass+deltam/2),Tc,Vol) - Ecv((mass-deltam/2),Tc,Vol))/deltam
END FUNCTION

FUNCTION DeDT(mass, Tc, Vol)
DECLARE DEF Ecv
LET deltaT = 0.1    !1/10 degree F
LET DeDT = (Ecv(mass,(Tc+deltaT/2),Vol) - Ecv(mass,(Tc-deltaT/2),Vol))/deltaT
END FUNCTION
```

```
FUNCTION DEevapDm(m, T, V)
DECLARE DEF Eevap
LET deltam = 0.000625     !1/100 ounce
LET DEevapDm = (Eevap((m+deltam/2),T,V) - Eevap((m-deltam/2),T,V))/deltam
END FUNCTION

FUNCTION DEevapDt(m, T, V)
DECLARE DEF Eevap
LET deltaT = 0.1     !1/10 degree F
LET DEevapDt = (Eevap(m,(T+deltaT/2),V) - Eevap(m,(T-deltaT/2),V))/deltaT
END FUNCTION

!*****************************************************************
!                    THERMODYNAMIC FUNCTIONS
!
FUNCTION quality(m, T, V)
DECLARE DEF vliq
DECLARE DEF vvap
LET quality = (V-m*vliq(T)) / ( m*(vvap(T)-vliq(T)) )
END FUNCTION

FUNCTION Psat(T)
!gives saturation pressure in psia, T in F
LET Psat = 23.932968228 + 0.51418662707*T + 0.0037341886015*T^2 + 0.0000190658186*T^3
END FUNCTION

FUNCTION hliq(T)
!gives enthalpy in BTU/lb, T in F, for saturated liquid
LET hliq = 8.536860812 + 0.2177245061*T - 0.000011400220011*T^2 + 0.0000087534587076*T^3
END FUNCTION

FUNCTION hvap(T)
!gives enthalpy in BTU/lb, T in F, for saturated vapor
LET hvap = 77.252285672 + 0.10468129772*T + 0.000022011282416*T^2 - 0.00000087986314726*T^3
END FUNCTION

FUNCTION uliq(T)
!gives internal energy in BTU/lb, T in F, for saturated liquid
LET uliq = 8.48644651 + 0.21641471052*T - 0.000012813919711*T^2 + 0.0000076402277996*T^3
END FUNCTION

FUNCTION uvap(T)
!gives internal energy in BTU/lb, T in F, for saturated vapor
LET uvap = 70.154332782 + 0.095941438918*T + 0.000047077025446*T^2 - 0.0000068031077878*T^3
END FUNCTION

FUNCTION vliq(T)
!gives saturated liquid volume in ft^3/lb, T in F
LET vliq = 0.011038151037 + 0.000013743768887*T - 0.000000095701304835*T^2 + 0.000000000036043141398*T^3
END FUNCTION

FUNCTION vvap(T)
!gives saturated vapor volume in ft^3/lb, T in F
LET a = 1.6248139964 - 0.032160201866*T + 0.00033008938409*T^2 - 0.0000017596245796*T^3
LET vvap = a + 0.000000000036691583966*T^4
END FUNCTION
```

```
FUNCTION density(T1, P1)
!returns density of slightly superheated vapor in lbs/ft^3
!used only in vapor mass flow rate calculation
LET R = 1.986/120.93
LET Z = 0.83
LET density = P1/(R*(T1+460)*Z)*144/778.2
END FUNCTION

FUNCTION SVapPres(m,T,V)
!returns the ideal gas pressure for slightly superheated vapor
!uses compressibility factor
!used in calculating the pressure in the consdenser after it's superheated
LET R = 1.986/120.93*778.2/144
LET Z = 0.83
LET rho = m/V
LET SVapPres = Z*rho*R*(T+460)
END FUNCTION

!*********************************************************************
!                    MASS FLOW RATE FUNCTIONS
!
FUNCTION mflow(P)
!mass flow rate in lbs per hour for liquid
LET mflow = 1.987-3.025*P/25+0.146*(P/25)^2
END FUNCTION

FUNCTION vapormdot(f, L, D, g, Pc, Pe,Tvap)
!Uses Newton Raphson subroutines to get the vapor mass flow rate
!Assumes fanno flow conditions
!Flow rate is in oz/min
DECLARE DEF density
DIM x(1),r(1),k(1)
LET niter=50          !  maximum number of Newton iterations allowed
LET toll=0.0000001    !  tol. for stopping iteration (see subroutine comments)
LET delta = .00000001 !  fractional increment for PD calculation.
LET nvar = 3
LET ncon = 6

MAT x=con(nvar)       !  x values set to 0, variables sent to Newton Raphson
MAT r=con(nvar)       !  r values set to 0, Residuals
MAT k=con(ncon)       !  k values set to 0, Constants sent to Newton Raphson

LET x(1) = .08        !  Mach # at inlet of cap tube, initial guess
LET x(2) = .9         !  Mach # at exit of cap tube, initial guess
IF Pc < 150 THEN LET x(2) = 0.5
IF Pc < 125 THEN LET x(2) = 0.4
IF Pc < 100 THEN LET x(2) = 0.3
IF Pc < 75 THEN LET x(2) = 0.2
IF Pc < 50 THEN
  LET x(2) = 0.1
  LET x(1) = 0.07
END IF
IF Pc < 40 THEN
   LET x(2) = 0.05
   LET x(1) = 0.04
END IF
```

```
IF PC < 30 THEN
   LET x(2) = 0.03
   LET x(1) = 0.02
END IF

LET x(3) = Pc - .5       !  Pressure at inlet of cap tube, initial guess

LET k(1) = f           !  Fills in constant array for equation solver
LET k(2) = L
LET k(3) = D
LET k(4) = g
LET k(5) = Pc
LET k(6) = Pe
LET MW = 120.93        !  mollecular weight of R12
LET Area = PI/4*D*D/144  !  cross sectional area of cap tube in ft^2

CALL nr(x,r,k,nvar,toll,niter,delta)       ! Newton Raphson Subroutine
LET P1 = x(3)
LET M1 = x(1)
LET T1 = (Tvap+460+5)/(1 + M1*M1*(g-1)/2) - 460
LET c = (g*1545/MW*32.174*(T1+460))^.5      !speed of sound in {ft/sec}
LET rho = density(T1, P1)
LET vapormdot = rho*M1*c*3600*Area*16/60
END FUNCTION



!*************************************************************************
!                       Subroutines from here on
!*************************************************************************

SUB nr(x(),r(),k(),nvar,toll,niter,delta)
   !    Generalized newton-raphson subroutine
   !    Numerical partial derivative version
   !    c o pedersen,  m&ie dept, u of illinois
   ! Inputs:
   !    x = variable array, should contain initial values on entry (nvar long)
   !    k = constant array
   !    nvar = number of variables
   !    toll = convergence criterion (toll*dot(x,x), suggest.001)
   !    niter = max number of iterations allowed
   !    delta = increment of x in partial deriv calc (suggest .001)
   ! Outputs:
   !    r = residual equation values
   !    x = final x values
   !    niter = actual number of iterations
   !  Required Subroutines:
   !       rcalc(r(),x(),k())  !  subroutine to evaluate residual
   !                     equations (supplied by user).
   !  Subroutines used:
   !       calcfp(r(),ro(),x(),k(),fprime(,),delta)1
   !       !  evaluates numerical partial derivatives
   !
   DIM dx(1),ro(1),fprime(1,1),invfprime(1,1)
   !  initialize, resize and zero arrays
   LET maxiter=niter           ! pass in max number of iterations, return actual number
   MAT r=zer(nvar)
```

```
   MAT dx=zer(nvar)
   MAT ro=zer(nvar)
   MAT fprime=zer(nvar,nvar)
   MAT invfprime=zer(nvar,nvar)
   FOR niter = 1 to maxiter
      CALL calcfp(r,ro,x,k,fprime,delta)
      CALL calcr(r,x,k)
      ! **
      ! **    solve for corrections
      ! **    note +r is used on rhs
      ! **    corrections will be subtracted from base value
      ! **
      MAT invfprime= inv(fprime)
      MAT dx=invfprime*r
      MAT x=x-dx
      LET err=dot(dx,dx)
      LET xnorm = dot(x,x)
      IF  err  < toll*xnorm  then    ! termination condition
        CALL calcr(r,x,k)           !reevaluate r
        EXIT SUB
      END IF
   NEXT niter
END SUB


SUB calcfp(r(),ro(),x(),k(),fprime(,),delta)
   ! **
   !  Subroutine to fill the partial derivative matrix (Jacobian)
   !
   !  The subroutine calls routine calcr to evaluate all derivatives.
   !  calcr must be given a set of variable (x) values.  It returns
   !  corresponding values for all the residual equations.
   !  It initially calculates a set of base values ro, based on the initial
   !   x vector supplied, and uses that set in all the partial derivative
   !   evaluations.
   !
   !  Note that it evaluates an entire column of the Jocobian when it has
   !   incremented one of the x values.  This helps to reduce the number of
   !   calculations for a sparce Jacobian.
   !
   !  The variable excursion for the PD calculation is delta (input) times the
   !   current value of the variable.
   !
   ! **
   LET nvar=size(x)
   CALL calcr(ro,x,k)
   FOR i=1 to nvar
      LET  deltax=delta*x(i)
      LET x(i)=x(i)+deltax
      CALL calcr(r,x,k)
      FOR  j=1 to nvar
         LET fprime(j,i)=(r(j)-ro(j))/(deltax)
      NEXT j
      LET x(i)=x(i)-deltax
   NEXT i
END SUB
```

```
SUB  CALCR(R(),X(),k())
   !-------------------------------------------------------
   ! **   SUBROUTINE TO EVALUATE RESIDUAL EQUATIONS
   !-------------------------------------------------------
   ! **   ASSIGN VALUES TO THE VARIABLES FROM
   ! **   THE X ARRAY TO SIMPLIFY CALLING PROCEDURE
   ! **   AND MAKE THE EQUATIONS READABLE


   LET f = k(1)
   LET L = k(2)
   LET D = k(3)
   LET g = k(4)
   LET Pc = k(5)
   LET Pe = k(6)

   LET M1 = x(1)
   IF M1 < 0.0001 THEN LET M1 = 0.0001
   LET M2 = x(2)
   LET P1 = x(3)
   !-------------------------------------------------------
   ! **  RESIDUAL EQUATIONS
   !-------------------------------------------------------
   LET R(1) = -f*L/D + (g+1)/(2*g)*log((1+(g-1)/2*M2^2)/(1+(g-1)/2*M1^2)) - (1/g)*(1/M2^2 - 1/M1^2)  -
(g+1)/(2*g)*log(M2^2/M1^2)
   LET R(2) = Pc - P1*(1+(g-1)/2*M1^2)^(g/(g-1))
   LET R(3) = Pe/P1 - M1/M2*((1+(g-1)/2*M1^2)/(1+(g-1)/2*M2^2))^.5
END SUB
```

Appendix D: Convective Heat Transfer in the Suction Line

One way to determine whether vapor alone could have achieved the rapid temperature drop of the suction line (during the first 30 seconds of the on-cycle for the 90 °F ambient case) is to compare the observed convection coefficient to the theoretical coefficient. The observed convection coefficient, h_{obs}, is determined from Equation D.1,

$$h_{obs} A \Delta T = \frac{dE}{dt} \qquad \text{D.1}$$

where A is the internal surface area of the suction line (40.3 in^2), ΔT is the average temperature difference between the suction line surface and the refrigerant (22 °F), and E represents the energy stored in the interchanger. ΔT is determined by averaging the measured temperature differences at both ends of the suction line over time. The amount of energy transferred from the interchanger (for the first 30 seconds of the on-cycle) was estimated to be 1 Btu in Chapter 6, thus the average rate that energy was removed is 1/30 Btu/sec, or 120 Btu/hr. Using these values, Equation D.1 is solved to find that h_{obs} is 19.5 Btu/hr-ft^2-°F.

The Dittus-Boelter equation, Equation D.2,

$$\frac{h_{DB} D}{k} = 0.023 Re^{0.8} Pr^{0.4} \qquad \text{D.2}$$

can be used to calculate the theoretical heat transfer coefficient for vapor flow through the suction line, h_{DB}. All refrigerant properties are calculated for superheated vapor at the average refrigerant temperature. Definitions for the Reynolds number, Re, and the Prandtl number, Pr are provided by Equations D.3 and D.4 respectively.

$$Re = \frac{4\dot{m}}{\pi D \mu} \qquad \text{D.3}$$

$$Pr = \frac{\mu c_p}{k} \qquad \text{D.4}$$

Descriptions and values for all parameters are found in Table D.1. Using these values, h_{DB} is calculated to be 19.2 Btu/hr-ft^2-°F.

Table D.1 Dittus-Boelter parameter values

Parameter	Description	Value
D	suction line inside diameter	0.2565 in^2
k	thermal conductivity of R-12	0.00463 Btu/hr-ft-°F
$\dot{m}$	typical mass flow rate	15 lb/hr
μ	viscosity	0.02718 lb/ft-hr
c_p	specific heat	0.14596 Btu/lb-°F
Re	Reynolds number	32,874
Pr	Prandtl number	0.8568

The theoretical and measured convection coefficients are extremely close, confirming that vapor alone could have caused the rapid temperature drop of the suction line during the first 30 seconds of the on-cycle.

Appendix E: Compressor Power Measurement

Compressor calorimetry data are customarily taken in a 90 °F ambient room with the suction gas maintained at 90 °F. A curve fit for compressor power is usually made from this data as a function of condensing and evaporating temperatures alone. Under different ambient conditions, the inlet temperature varies, thus the density of the suction gas varies as well. This can have a significant impact on the performance of the compressor. This effect has been recognized by Dabiri and Rice (1981) who have proposed correction factors to account for different levels of superheat at the compressor inlet.

Figures E.1 and E.2 compare the measured compressor power with the power predicted by the compressor map for two separate steady state data sets. The compressor map power, P_{comp}, is given in Equation E.1:

$$\begin{aligned} P_{comp} = \quad & (2.1156e2 + 2.5026*T_{evap} + 9.699e\text{-}3*T_{evap}^{\,2}) \\ + \quad & (-8.531e\text{-}2 - 3.445e\text{-}3*T_{evap} + 7.6403e\text{-}5*T_{evap}^{\,2})*T_{cond} \\ + \quad & (2.477e\text{-}3 + 8.8393e\text{-}5*T_{evap} + 1.9133e\text{-}7*T_{evap}^{\,2})*T_{cond}^{\,2} \end{aligned} \qquad \text{E.1}$$

where T_{evap} is the saturation temperature at the measured compressor inlet pressure, and T_{cond} is the saturation temperature at the measured compressor exit pressure.

The data are arranged such that points with the same ambient temperature are grouped together. For both data sets, the compressor map power and the measured power agree best for the 90 °F ambient data points. For the 60 °F and 75 °F ambient data, the compressor map is consistently 9 W and 2 W lower than the measured power respectively. For the 100 °F ambient data, the compressor map is 4W higher than the measured power.

Different ambient temperatures obviously affect the performance of the compressor, rendering the map inaccurate. The ambient temperature has several effects on the compressor. First, a lower ambient temperature lowers the shell temperature. It was shown in Chapter 2 that the compressor heat rejection rate, Q_{comp}, is linearly related to the difference in temperature between the compressor shell and its surroundings. Further investigations should be made concerning the effect of Q_{comp} on power consumption. Different operating temperatures may also affect the performance of the compressor motor, as individual components change temperature and mechanical clearances change. Second, at lower ambient temperatures, the pressure ratio across the compressor is lower, thus decreasing the electric motor load. Since electric motors usually have lower efficiencies at reduced loads, this tends to reduce the overall compressor efficiency. Finally, the suction gas becomes cooler and denser at lower ambient temperatures, which may also affect the compressor power requirements. For modeling purposes, a correction should be developed for the compressor map that accounts for these effects. An experiment should be designed which could vary shell temperature and suction gas temperature to determine the importance of these factors.

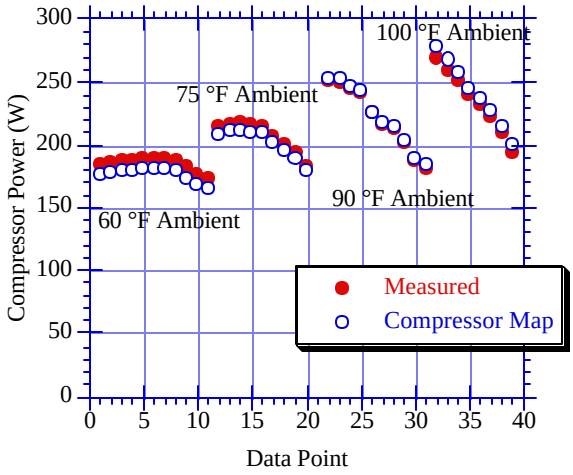

Figure E.1 Measured vs. predicted compressor power for fall 1992 data

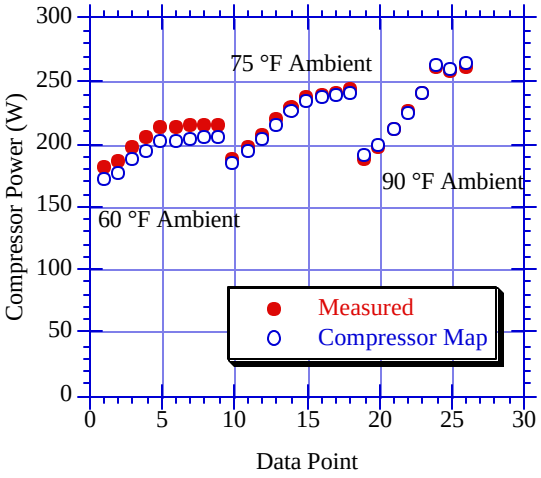

Figure E.2 Measured vs. predicted compressor power for spring 1993 data